Physics in Medicine & Biology

TOPICAL REVIEW

Review on biophysical modelling and simulation studies for transcranial magnetic stimulation

IOP Publishing Phys. Med. Biol. 65 (2020) 24TR03 https://doi.org/10.1088/1361-6560/aba40d

Physics in Medicine & Biology

IPEM Institute of Physics and Engineering in Medicine

RECEIVED
17 March 2020

REVISED
19 June 2020

ACCEPTED FOR PUBLICATION
8 July 2020

PUBLISHED
3 December 2020

TOPICAL REVIEW

Review on biophysical modelling and simulation studies for transcranial magnetic stimulation

Jose Gomez-Tames[1,3], Ilkka Laakso[2] and Akimasa Hirata[1,3,4]

[1] Nagoya Institute of Technology, Department of Electrical and Mechanical Engineering, Nagoya, Aichi 466-8555, Japan
[2] Department of Electrical Engineering and Automation, Aalto University, FI-00076, Finland
[3] Center of Biomedical Physics and Information Technology, Nagoya Institute of Technology, Nagoya 466-8555, Japan
[4] Fontier Research Institute for Information Science, Nagoya Institute of Technology, Nagoya 466-8555, Japan

E-mail: jgomez@nitech.ac.jp

Keywords: transcranial magnetic stimulation, dosimetry, multiscale modeling, electric field, neuron, anatomical human head model

Abstract

Transcranial magnetic stimulation (TMS) is a technique for noninvasively stimulating a brain area for therapeutic, rehabilitation treatments and neuroscience research. Despite our understanding of the physical principles and experimental developments pertaining to TMS, it is difficult to identify the exact brain target as the generated electric field exhibits a non-uniform distribution owing to the complicated and subject-dependent brain anatomy and the lack of biomarkers that can quantify the effects of TMS in most cortical areas. Computational dosimetry has progressed significantly and enables TMS assessment by computation of the induced electric field (the primary physical agent known to activate the brain neurons) in a digital representation of the human head. In this review, TMS dosimetry studies are summarised, clarifying the importance of the anatomical and human biophysical parameters and computational methods. This review shows that there is a high consensus on the importance of a detailed cortical folding representation and an accurate modelling of the surrounding cerebrospinal fluid. Recent studies have also enabled the prediction of individually optimised stimulation based on magnetic resonance imaging of the patient/subject and have attempted to understand the temporal effects of TMS at the cellular level by incorporating neural modelling. These efforts, together with the fast deployment of personalised TMS computations, will permit the adoption of TMS dosimetry as a standard procedure in medical applications.

1. Introduction

Transcranial magnetic stimulation (TMS) is a technique for noninvasively stimulating a target area of the brain. TMS is used for diagnosis in pre-surgical identification of motor and language functions and in the treatment of neurological diseases or conditions. Since the first study on TMS (Barker *et al* 1985), this field has grown substantially. One difficulty is the lack of available biomarkers to investigate the effects of TMS in the various regions of the brain, excluding the somatosensory, visual, and language regions. Moreover, recent studies report that the electric field (EF) in the brain exhibits a non-uniform distribution owing to the complicated and subject-dependent brain anatomy (Thielscher *et al* 2011, Janssen *et al* 2013, Nummenmaa *et al* 2013, Laakso *et al* 2014), which results in a greater challenge while estimating the target regions. Further, the estimated regions by TMS may vary according to different parameters, such as the variations in the type of magnetic coil, its position and orientation over the scalp, and the current waveform injected into the coil (Taniguchi *et al* 1993, Terao and Ugawa 2002, Holsheimer *et al* 2007). Thus, the necessity to understand, visualise, and individually optimise the TMS dosage in the brain has motivated the application of computational dosimetry.

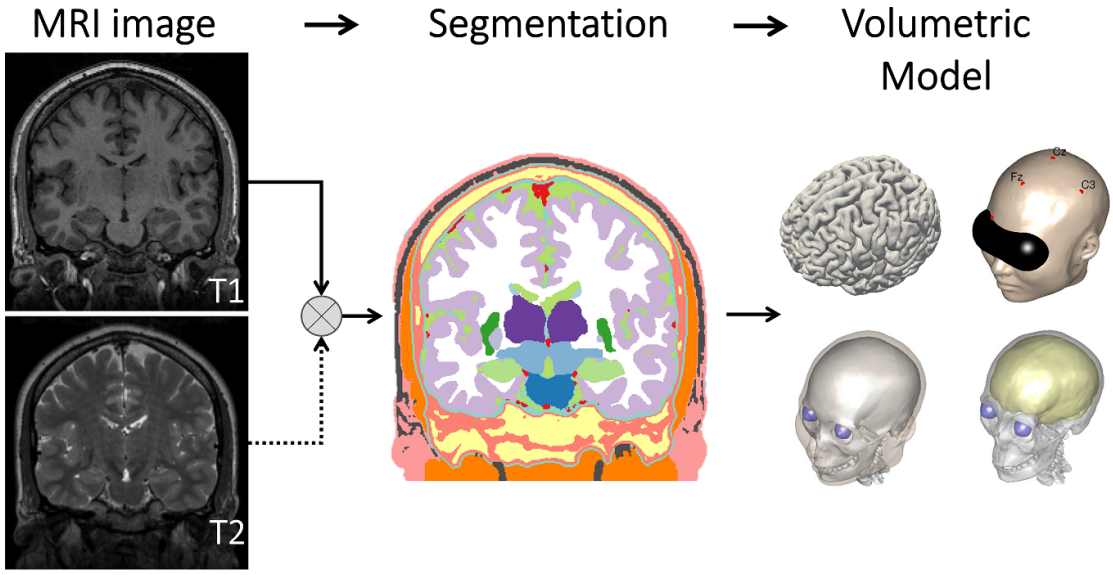

Figure 1. Pipeline example of the generation of individualised head models from magnetic resonance images.

For the past 30 years, computational dosimetry has progressed significantly in biophysical and electrophysiological modelling techniques to investigate the effects of electromagnetic fields in the human body. In TMS, the primary physical agent known to activate neurons is the induced EF; moreover, recent studies have enabled the prediction of the stimulation location and optimised the dosages of the stimulation parameters (Opitz *et al* 2014, Aonuma *et al* 2018, Seynaeve *et al* 2019, Weise *et al* 2020). These procedures estimate the EF in the brain while considering the effects of the various physical aspects involved in TMS (e.g. biological tissue conductivity, coil design, head anatomy). Recent studies considered the connection between induced EF and neuronal responses, which was based on a three-staged computation. The first step (subsection 2.1) involves expressing a human body as discrete geometric elements with millimetre or sub-millimetre resolution based on medical images. The second step (subsection 2.2) is the determination of the induced EF in the brain. The third step (subsection 2.3) involves modelling the neural responses evoked by TMS at the cellular level.

Reviews and guidelines for TMS were published from the clinical perspective (Rossi *et al* 2009, Perera *et al* 2016). However, no TMS review has been published on the simulation techniques for biophysical modelling to the best of our knowledge, despite the rapid increase in the number of computational studies. The current review presents the historical and most recent efforts on TMS modelling in humans. This review is intended for research groups working on dosimetry for clinical applications and researchers working on the clinical and neuroscience aspects of TMS, who are interested in adopting computational models.

2. Outline of computational models

TMS-induced EF is computed by using a realistically segmented human head model that represents the tissue-dependent conductivity distribution. The general pipeline for TMS modelling in an individualised head model is illustrated in figures 1 and 2. Further, the EF effects on a neuronal model can be investigated by using a compartmentalised cable equation, as shown in figure 3. The outline of the implementation process is described in the following subsections.

2.1. Development of a personalised head model

The construction of a human body model has progressed corresponding to the developments and improvements in medical images and their processing. In the 1990 s and early 2000 s, when image processing performance was inadequate, a certain amount of manual assessment was required for human tissue classification to construct human body models. The models were presented (Zubal *et al* 1994, Dimbylow 1997, Nagaoka *et al* 2004) as voxel phantoms and subsequently expanded to 'families' or 'populations' of phantoms (Christ *et al* 2010, Wu *et al* 2012, Park *et al* 2018). In the last 10 years, it has become possible to construct personalised head models almost automatically from magnetic resonance imaging (MRI) data, owing to progress in medical imaging techniques (Dale *et al* 1999, Fischl 2012, Windhoff *et al* 2013, Laakso *et al* 2015, Lee *et al* 2016, Huang *et al* 2019).

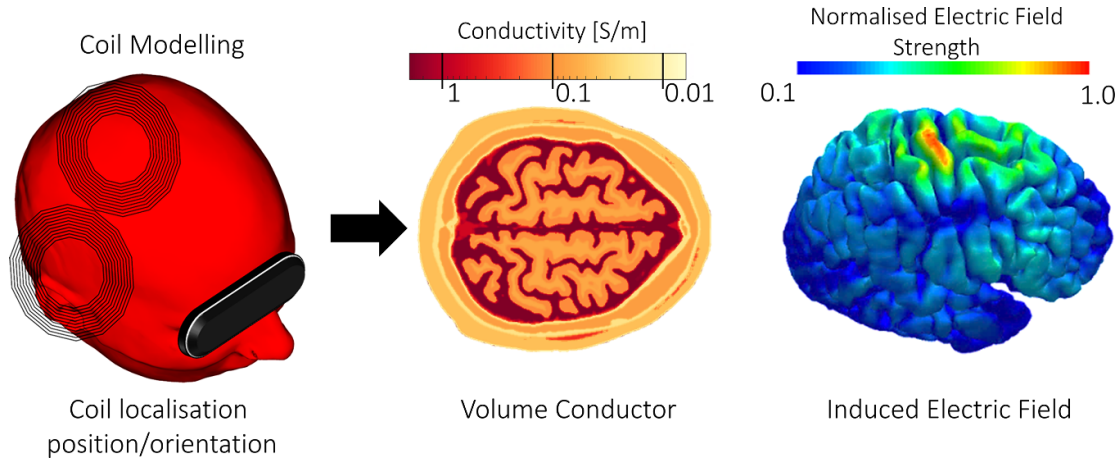

Figure 2. Electromagnetic computation pipeline. The TMS coil design is based on a realistic coil and the localisation and position can be retrieved from a neuro-navigation system when investigated together with neurophysiological measurements such as motor-evoked potential (MEP). The volume conductor is obtained by assigning the tissues conductivity to the digital head model from the pipeline in figure 1. Finally, the numerical computation yields the induced electric field (EF) in the brain.

Automatic segmentation of the brain and non-brain tissues from MRI data can be obtained using different image analysis software, such as FreeSurfer (Dale *et al* 1999, Fischl 2012), Statistical Parametric Mapping (SPM) (Ashburner and Friston 2005), and FMRIB software library (FSL) (Smith 2002). These different image analysis tools have been incorporated into different head model generation and EF calculation pipelines, such as ROAST (Huang *et al* 2019) and SimNIBS (Windhoff *et al* 2013). An illustration of a pipeline to segment the brain and non-brain tissues is shown in figure 1 (Windhoff *et al* 2013, Laakso *et al* 2015, Huang *et al* 2019).

2.2. Electromagnetic computation

Computational electromagnetic methods are based on the quasi-static approximation to determine induced EF at frequencies lower than several megahertz (Barchanski *et al* 2005, Hirata *et al* 2013), as shown in figure 2. In the quasi-static approximation, Maxwell's equations can be simplified by ignoring propagation, capacitive, and inductive effects (Plonsey and Heppner 1967, Jackson and Fox 1999), which result in the following equation for the electric scalar potential:

$$\nabla \cdot \left[\sigma \left(-\nabla \varphi - \frac{\partial}{\partial t} \boldsymbol{A}_0 \right) \right] = 0 \tag{1}$$

where $\{\boldsymbol{A}\_0\}$ and σ denote the magnetic vector potential of the applied magnetic field and the tissue conductivity, respectively. If the induced current marginally perturbs the external magnetic field, then $\{\boldsymbol{A}\_0\}$ is equal to the magneto-static vector potential that is completely decoupled from the EF and can be calculated by considering the Biot–Savart law pertaining to the source current distribution. At the boundary of the body, the scalar potential satisfies the Neumann boundary condition:

$$\mathbf{n} \cdot \nabla \varphi = -\mathbf{n} \cdot \frac{\partial}{\partial t} \boldsymbol{A}_0 \tag{2}$$

where **n** is a normal vector to the body surface.

Once equation (1) is solved, the induced EF **E** can be expressed as

$$\boldsymbol{E} = -\nabla \varphi - \frac{\partial}{\partial t} \boldsymbol{A}_0 \tag{3}$$

The factor $\partial \boldsymbol{A}_0 / \partial t$ is called the primary EF, which is induced by the changing magnetic field, which depends only on the TMS coil characteristics. The factor $-\nabla \varphi$ is called the secondary field, which is caused by charges in the conducting medium. The induced current density and EF can be related in terms of $\boldsymbol{J} = \sigma \boldsymbol{E}$. Equation (1) typically has no analytical solution. Instead, numerical methods must be used to approximate φ. Several computational electromagnetic methods can be applied to solve equation (1) including finite element method (FEM), boundary element method (BEM), and finite-difference method (FDM).

In the FEM, the geometry of the computation domain, in this case, the head, is divided into a mesh of several small non-overlapping finite elements, typically tetrahedrons or hexahedrons. Then, the mesh is used

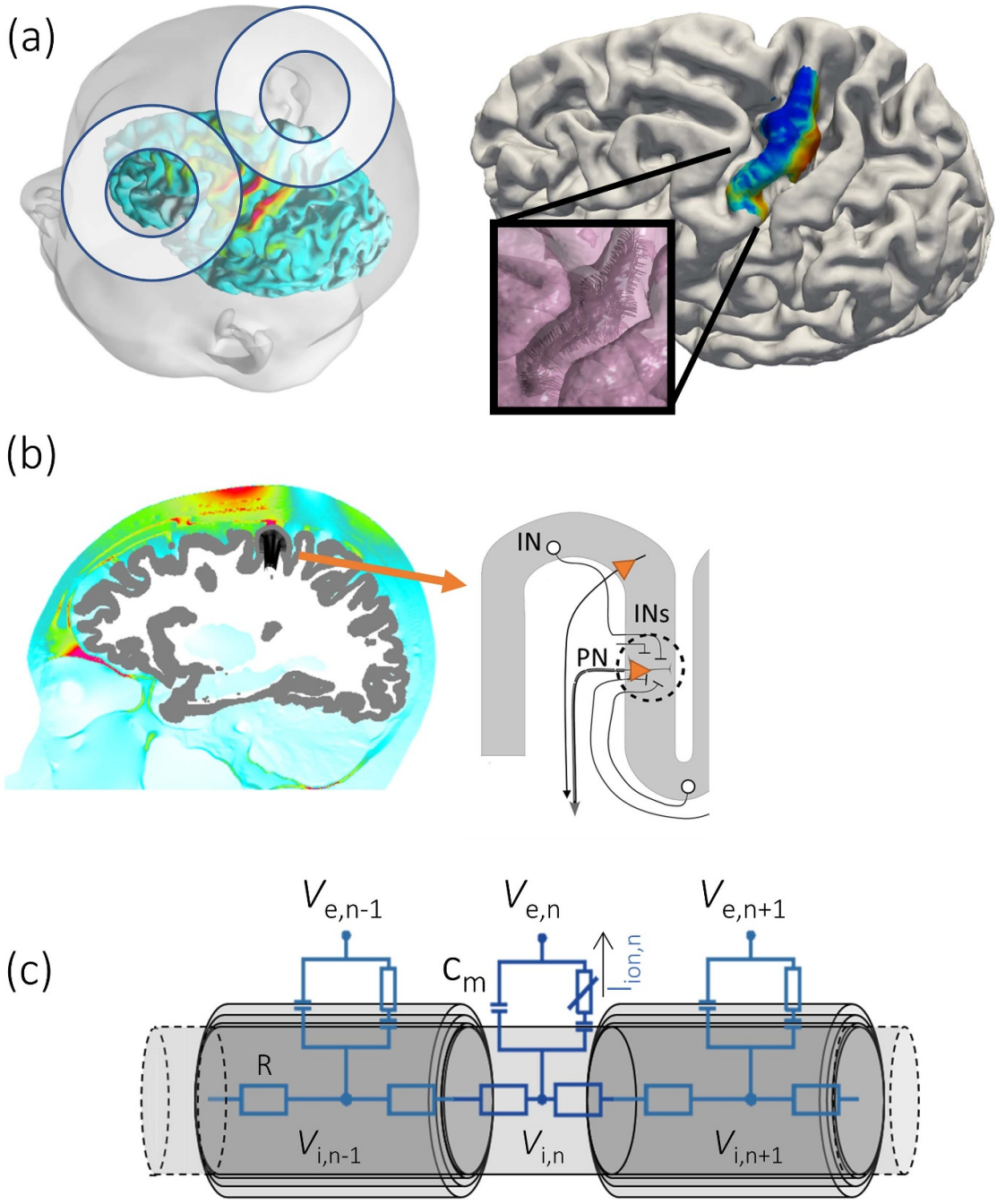

Figure 3. Multiscale modelling: (a) Transcranial magnetic stimulation (TMS)-induced EF drives neural activation; (b) TMS acts stronger on the neurons in the neocortex. Neurons are arranged in horizontal layers with different cell types and neural connections that can project to other areas of the brain regions (e.g. connection between interneurons IN and pyramidal neurons PN) or spinal cord; (c) cable equation that is coupled with the TMS-induced EF that represents a myelinated axon. The structure can be extended to consider more complicated morphologies such as bifurcations in the dendrites.

to define a set of basis functions, which are non-zero only in a small number of elements and are polynomials of a specified order inside each element. The approximate solution to equation (1) is calculated as a linear combination of these basis functions by solving a large linear equation system.

BEMs are derived by converting equation (1) to an integral equation form. The integral equation can be formulated using either the induced scalar potential (e.g. Ferguson and Stroink 1997) or the induced surface charge (e.g. Makarov *et al* 2018) as the unknown. If the geometry consists of a finite number of compartments, each having a uniform conductivity, the problem reduces to solving the unknown surface potential or charge on each interface between the compartments. In TMS literature, the tissue interfaces are commonly referred to as 'layers'. The integral equation for the surface potential/charge is solved numerically using the FEM. Subsequently, the surface potential/charge can be used to calculate the induced potential and EF at any location.

FDM formulations are derived by replacing the spatial derivatives in equation (1) by their finite-difference approximations, which results in a linear equation system from which the unknown potential values at each element can be obtained. FDM resembles the FEM in the special case of a structured mesh consisting of hexahedral elements. An example of FDM is the scalar potential finite difference (SPFD) method (Dawson and Stuchly 1996), which uses the second-order central difference approximation to the left side of equation (1).

Each method has advantages and disadvantages when it comes to modelling TMS. FEM and BEM can use unstructured computational meshes that can accurately represent curved boundaries between tissues. The mesh can furthermore be locally refined near the targeted brain areas, thereby improving accuracy (Windhoff *et al* 2013). The weakness of unstructured meshes is that the generation of a good quality mesh from the segmented MRI data is a non-trivial task. In contrast, FDM is limited to a structured rectangular grid, which is trivially obtained from the segmented images, but results in 'staircase' approximation of curved boundaries. FEM approaches that use structured grids also suffer from the staircase approximation error. BEM differs from FEM and FDM as it only requires the meshing of the boundaries between the tissue compartments. Each compartment must have a uniform conductivity; consequently, the method cannot efficiently model anisotropic or heterogeneous materials, which can be modelled using FEM or FDM in a straightforward manner (Wang and Eisenberg 1994, Windhoff *et al* 2013).

Gomez *et al* (2020) compared the accuracy of FEM, BEM, and FDM for modelling TMS-induced EFs in a realistic head model. Using computational meshes of varying resolutions as well as basis functions of different polynomial orders, they showed that all three methods could produce accurate results, provided that the resolution of the computational mesh was sufficiently fine. To obtain a desired level of numerical accuracy, the required mesh resolution depended on the method and the order of the elements.

Saturnino *et al* (2019) and Soldati and Laakso (2020) obtained similar results, showing how the error in the EFs calculated using the FEM diminished when the resolution of the mesh (tetrahedral or cubical elements) was refined. These findings indicate that the numerical errors can be controlled. Therefore, all computational methods, if their parameters have been set appropriately, can produce sufficient computational accuracy for TMS modelling studies.

2.3. Multiscale model incorporating neural modelling

A cable equation is used to describe propagation and interaction of electrical signals in the axons of neurons, as shown in figure 3. Further, it can incorporate the ionic mechanisms underlying the initiation and propagation of action potentials. Hodgkin and Huxley proposed the first model for neural signal propagation in a squid giant axon (Hodgkin and Huxley 1952). The seminal study resulted in the development of subsequent models of excitable cell membrane (Frankenhaeuser and Huxley 1964, Chiu and Ritchie 1979, Sweeney *et al* 1987, McIntyre *et al* 2002) including single compartmental models of cells in the brain cortex (Aberra *et al* 2018). The original cable equation was initially modified to include responses to electric and magnetic stimulation (McNeal 1976, Rattay 1986, Reilly 1989, Roth and Basser 1990); this allowed examinations of the spinal cord, muscle, and brain stimulation using realistic models (Doheny *et al* 2008, Wongsarnpigoon and Grill 2008, Danner *et al* 2011, Salvador *et al* 2011, Seo *et al* 2015, Aberra *et al* 2020).

A modified cable equation describes the neuronal membrane polarisation and activation due to TMS-induced EF:

$$c_m \frac{dV_m}{dt} = -I_{ion} + \frac{1}{R}\frac{d^2V_m}{ds^2} + \frac{1}{R}\frac{d^2V_e}{ds^2} \tag{4}$$

where c_m, R, and I_ion denote the membrane capacitance, the intra-axonal resistance, and the ionic current of the membrane per unit length, respectively. The spatial variable s is the distance along the trajectory of the neuron. The term V_m denotes the membrane potential along the cable, the quasi-potential V_e is the line integral of the induced EF:

$$V_e(s,t) = -\int_0^s \boldsymbol{E}(\boldsymbol{r}(s'),t)\cdot ds' \tag{5}$$

where $\boldsymbol{r}$ is the arc length parametrisation of the path of the neuron.

The cable equation (4) can be modelled in the compartmental form so that different sections of the neuron are approximated by an electric network. Each compartment n consists of axial resistance, membrane conductance, and capacitance. The membrane potential in each compartment can be determined from

$$c_{m,n}\frac{dV_{m,n}(t)}{dt} = -I_{ion,n} + \frac{V_{m,n-1}(t) - 2V_{m,n}(t) + V_{m,n+1}(t)}{R} - \frac{V_{e,n-1}(t) - 2V_{e,n}(t) + V_e(t)}{R} \tag{6}$$

Table 1. Head model representation by canonical or simplified geometries in various studies.

Author	Characteristics		
(a) Canonical			
Roth *et al* (2002)	Homogeneous sphere (7 cm)		
Miranda *et al* (2003)	Heterogeneous sphere (4.6 cm): CSF and other		
Thielscher and Kammer (2004)	Homogeneous sphere (8 cm)		
Salinas *et al* (2009)	Heterogeneous sphere (10 cm, 1 and 4 layers)		
Hernandez-Garcia *et al* (2010)	Homogeneous sphere (7.5 cm)		
Deng, Lisanby and Peterchev (2013, 2014)	Homogeneous sphere (8.5 cm)		
Nummenmaa *et al* (2013)	Homogeneous sphere (globally best-fitted to inner-skull surface) Homogeneous sphere (locally fitted to inner-skull surface close to TMS coil location)		
Koponen *et al* (2015)	Homogeneous sphere (8.5 cm)		
Yamamoto *et al* (2016)	Homogeneous sphere (7.5 cm)		
Wei *et al* (2017)	Homogeneous sphere (8.5 cm)		
(b) Simplified	Characteristics	Acquired method	No subjects
Thielscher and Kammer (2002)	Sphere manually fitted to the inner surface of the skull	1.5 T MRI (T1)	Four subjects (25–38 y.o., one female)
Kim *et al* (2006)	Norman model (homogeneous)	N.A	One male (age N.A)
Silva *et al* (2008)	Idealised gyrus-sulcus	N.A	N.A
Salvador *et al* (2009)	Head-shaped homogeneous	MRI	One subject (gender and age N.A)
Stokes *et al* (2013)	Head-shaped homogeneous	Phantom (IEEE 1528–2003)	N.A
Yamamoto *et al* (2015)	Anatomical brain	Phantom (NICT)	One male, 22 y.o.
Sekino *et al* (2015)	Anatomical brain	MRI	One (gender and age N.A)

DTI: refers to diffusion tensor imaging.

Finally, it is to be noted that the electrical properties of each compartment depend on the neuron segment, so the model can be extended to include morphologically detailed neurons for the central nervous system (CNS) (Aberra *et al* 2018). The model can consist of bifurcations and branches, pre- and post-synaptic terminals, and dendritic arborisation.

3. Electric field dosimetry

In the early 1990 s, it was possible to calculate the EF strength using spherical models of the brain (Cohen *et al* 1990, Tofts 1990, Eaton 1992). However, the location and extent of the EFs are affected by anatomical factors (e.g. gyrification) and the electrical conductivities of different tissue types, which can only be accounted for using anatomical models. The progress of TMS dosimetry is summarized in figure 4 that shows the transition from simplified to anatomical models. Simplified head models are listed in table 1, and complexity variation of the anatomical head model and its targets (population segments and brain regions) are summarised in figure 5.

In this section, subsections 3.1–3.4 deal with fundamental aspects of TMS modelling, such as modelling of the anatomy, electrical conductivity and magnetic coils, whereas subsections 3.5–3.8 deal with TMS dosimetry applications, such as coil design optimisation, guiding TMS dose, and comparison of EF dosimetry with experimental measurements. The identified studies in this review are based on a search strategy presented in appendix A that was developed for each subsection. For this we focus on human dosimetry studies. Finally, the data used in figure 5 was retrieved from the identified studies in subsections 3.1 and 3.5–3.8. In the case of table 1, the data was retrieved from studies in subsections 3.1 and 3.3–3.6.

3.1. Representation of head tissues

The initial attempts to compute the TMS-induced EF used the brain representations as an infinite half-space or as spheres. However, as illustrated in figure 6, the lack of anatomical detail limits the accuracy of the estimated EF. The following seven studies that investigated the effects of tissue representation on the induced EF were identified.

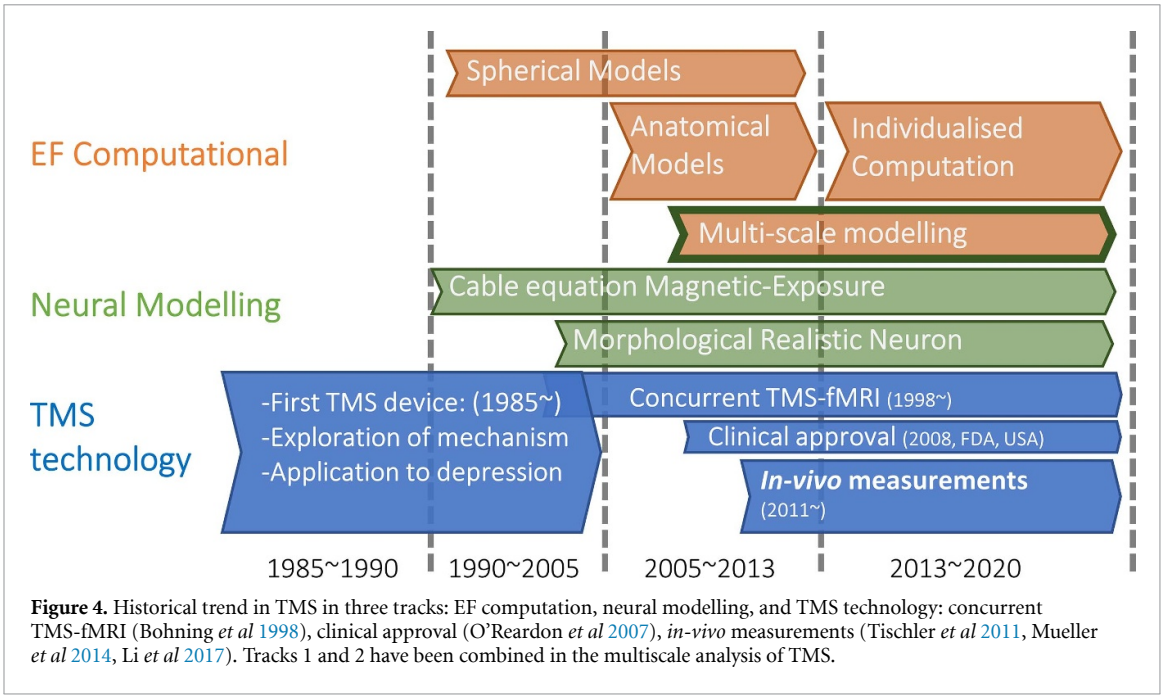

Figure 4. Historical trend in TMS in three tracks: EF computation, neural modelling, and TMS technology: concurrent TMS-fMRI (Bohning *et al* 1998), clinical approval (O'Reardon *et al* 2007), *in-vivo* measurements (Tischler *et al* 2011, Mueller *et al* 2014, Li *et al* 2017). Tracks 1 and 2 have been combined in the multiscale analysis of TMS.

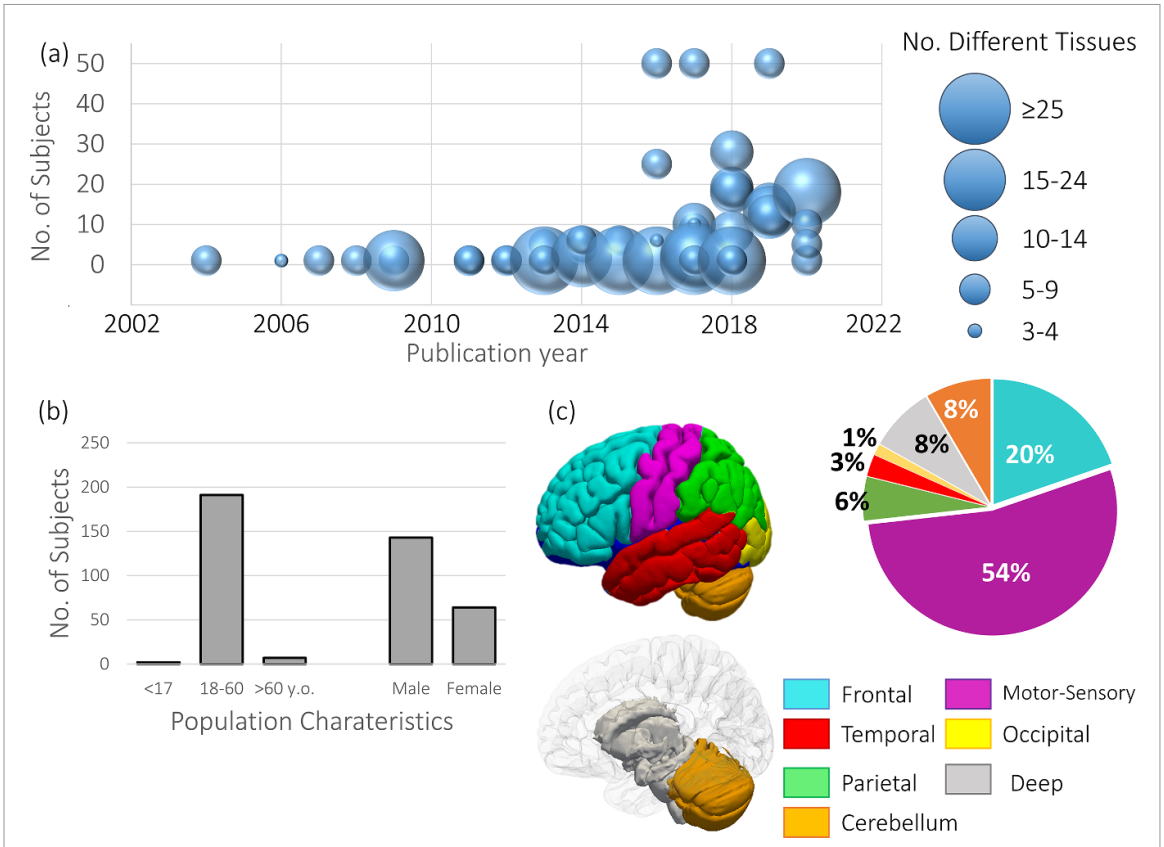

Figure 5. Anatomical head models in TMS: (a) Evolution of head model representation complexity; (b) number of subjects according to age and gender; (c) number of studies based on target brain region.

Wagner *et al* (2004) considered a heterogeneous model (five-layered model) to investigate the effects of tissue inhomogeneity and geometry on the induced current density using the FEM. Their study showed that the boundaries between tissues of different conductivities strongly affected the distribution of the current density. In particular, tissue inhomogeneity produced a normal component of the current density, which is absent in spherical head models and which was equivalent to 30% of the total current density at the target region.

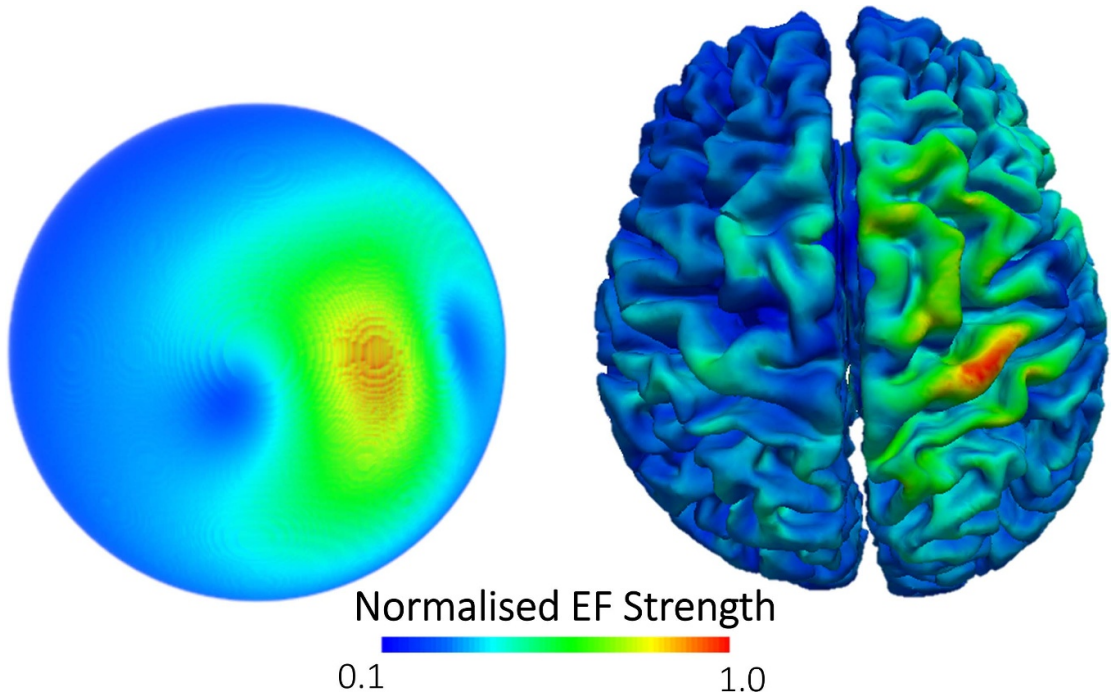

Figure 6. Illustration of TMS-induced EF in spherical and anatomical head models using figure-of-eight coil. The EF is shown in the brain cortex.

Toschi *et al* (2008) used a realistic heterogeneous head model, which was derived from MRI data, and computed the induced EF using FDM. They demonstrated that TMS with a symmetrical distribution of the primary field, such as in a figure-of-eight coil, induces a highly asymmetrical EF distribution in a realistic anatomy. The authors concluded that a high-resolution field solver and a realistic reconstruction of the head geometry of the subject are required for a highly accurate prediction of the induced EF.

Salinas *et al* (2009) used a realistic six-layer head model to assess the effect of multiple layers on the EF strength using the BEM. The secondary EF is important as its strength ranges from 20%–35% of that of the primary EF. The authors concluded that an accurate tissue geometry representation is required to consider the secondary EF effects accurately.

Silva *et al* (2008) considered tissue heterogeneity in a layered cortical sulcus model to investigate the spatial distribution of the induced EF. The primary finding was that the electrical conductivity and cortical folding should be considered to estimate stimulation regions.

Thielscher *et al* (2011) used the FEM to characterise the induced EF in a head model that considered the realistic gyrification patterns. Five tissue types were considered. The induced EF strength in grey matter was increased by up to 50% when the induced current was perpendicular to the local gyral orientation in comparison with a simplified homogeneous model that neglected cortical gyrification. In contrast, the EF direction was predominantly influenced by the CSF-skull boundary. In general, when compared to the anatomical model, the spherical head model presented lower maximal field strengths, lower focality of the field in grey matter and did not show variation of the EF spatial distribution with changes of the TMS coil orientation.

Nummenmaa *et al* (2013) compared different head models with different levels of detail: spherical, semi-anatomical (skin, skull, and intracranial without CSF or gyrification), and anatomical (skin, skull, CSF, and brain) using the BEM. The results showed that anatomical and semi-anatomical head models demonstrated similar induced EF distributions, although the former had higher EF strength. In contrast, the spherical model did not reproduce distribution similar to the anatomical model.

Janssen *et al* (2014) incorporated geometrical detail, specifically for a highly detailed CSF-grey matter boundary in an FEM model. They concluded that omitting the secondary field due to charge accumulation at the boundaries of the tissue significantly affects the total induced EF distribution and strength.

In summary, heterogeneous anatomical head models are required for the accurate estimation of the induced EF (Wagner *et al* 2004, Silva *et al* 2008, Thielscher *et al* 2011, Janssen *et al* 2014, Bungert *et al* 2017). The boundaries between tissues of high contrast conductivities can strongly affect the induced EF distribution On the other hand, homogeneous models cannot describe the effects of coil orientation dependency, and the secondary field effects are omitted; consequently, the induced EF distribution is not

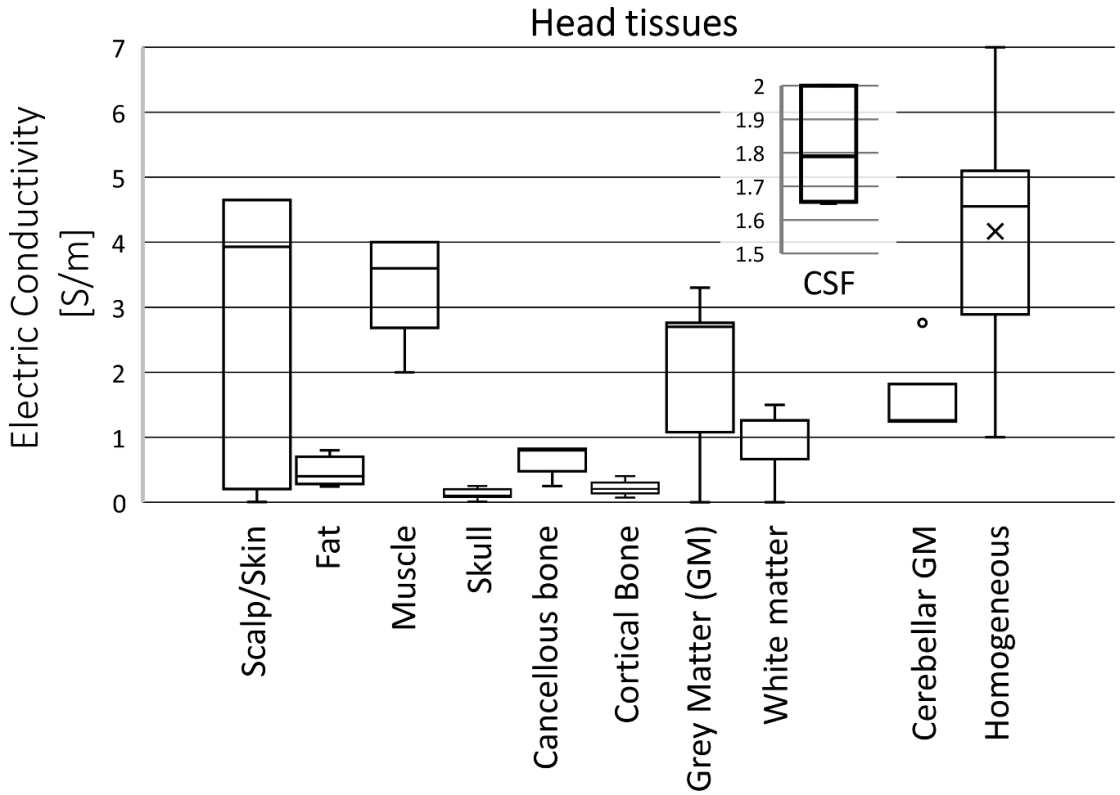

Figure 7. Box plot distribution of the conductivity values of the most common tissues used across different TMS dosimetry studies.

accurately predicted (Toschi *et al* 2008, Salinas *et al* 2009, Nummenmaa *et al* 2013, Janssen *et al* 2014, Bungert *et al* 2017).

3.2. Electrical conductivity: variability

The selection of the electrical conductivity of the tissues is a challenge, and it is sometimes a controversial topic owing to the lack of defined values and diversity of reported values (Saturnino *et al* 2019). Their selection becomes important as high contrast conductivity between neighbouring tissues significantly affects induced EF distribution, as discussed in the previous subsection. Here, we initially reviewed the variability of electrical properties of the tissues used in TMS modelling studies. In total, 66 modelling studies were identified; the reported conductivities values are summarized in figure 7.

The choice of the conductivity values is predominantly based on the conductivity values selected by Wagner *et al* (2004) or the tissue dielectric property database presented by Gabriel *et al* (1996) at the frequency of the TMS pulse (i.e. the inverse of pulse duration: 2.5 to 10 kHz).

The conductivity of CSF is relatively constant across different studies (1.65 to 2.0 S m^{-1}). The grey matter and white matter have relatively small variations, i.e. between 0.1 to 0.276 S m^{-1} and 0.07 to 0.126 S m^{-1}, respectively. These differences may not be significant in the localisation of the highest EF strengths in the cerebral cortex, according to Aonuma *et al* (2018) and Gomez-Tames *et al* (2018).

Scalp and skull present larger variabilities. The variability of the former is between 0.0002 to 0.465 S m^{-1}, and the latter between 0.001 to 0.08 S m^{-1}. In the case of the scalp, the innermost and outermost layers of the skin present large differences. The lower bound (0.0002 S m^{-1}) may be related to the outermost stratum corneum layer of the skin (Yamamoto and Yamamoto 1976). The upper bound (0.465 S m^{-1}) is based on the measurements at direct current (Burger and Milaan 1943). Certain studies adopted an average value between the fat (0.02 to 0.08 S m^{-1}) and muscle (0.2 to 0.4 S m^{-1}) when they considered them together as the scalp layer, such as Bungert *et al* (2017) or non-uniform values within the same tissue (Rashed *et al* 2020a). Although these non-brain tissues (except the CSF) do not significantly affect the TMS-induced EF on the brain tissues (Saturnino *et al* 2019), non-brain tissues are required to investigate the side-effects and safety.

3.3. Electrical conductivity: anisotropy

Anisotropic electrical characteristics of the brain, in particular the white matter, may affect the modelled EF. In the white matter, owing to the presence of interconnecting neural tracts, the conductivity in directions

along and across the neural tracts may differ by a factor of ten (Nicholson 1965). Four studies were identified that investigated the effect of anisotropy on the induced EF.

Miranda *et al* (2003) showed a significant difference in the induced EF when considering anisotropic conductivity in a heterogeneous spherical model using the FEM.

De Lucia *et al* (2007) used a realistic head model that considered anisotropic conductivity derived from diffusion tensor imaging in the brain. The induced EF in the part of the grey matter was marginally affected by the tissue anisotropy in an FEM model. Instead, the induced EF strength variations were approximately 10% between models using isotropic or anisotropic conductivity in the white matter.

Opitz *et al* (2011) showed that considering an anisotropic brain tends to enhance the local EF hotspots in white matter by 40% in an FEM model; however, no changes were observed in the grey matter.

De Geeter *et al* (2012) investigated the effect of realistic dispersive anisotropic tissue properties on the induced EF in a head model with realistic geometry using an FDM (impedance method). The results showed that anisotropy yields a difference of up to 19% on the maximum EF in the white matter (a mid-value between two previous studies (De Lucia *et al* 2007, Opitz *et al* 2011)), while the differences in the other tissues were not significant.

3.4. TMS coil models and verification

The accuracy of the TMS-induced EF depends on the level of detail of the magnetic coil. Three primary approaches have been used: modelling the coil as a collection of thin wires (Eaton 1992), magnetic dipoles (Ravazzani *et al* 1996), or realistic models that consider the current distribution in the coil windings (Salinas *et al* 2007). Verification of the correct modelling can be conducted by direct measurements of the induced EF in experimental phantoms. Seven studies that have considered these approaches for TMS coil modelling have been identified.

Thielscher and Kammer (2004) computed the induced EF by the superposition of the fields of magnetic dipoles that were placed using x-ray images of magnetic coils, extending the method presented by Ravazzani *et al* (1996).

Salinas *et al* (2007) presented a detailed TMS coil wiring geometry, which considered the width, height, shape, and number of turns of the wire. The induced EF computed using a detailed TMS coil model had an error within 0.5% with respect to the measurement values. A realistic approximation of the TMS coil model is more important to compute the EF near the coil than at the cortical depth, where no significant difference was measured between simple (thin wire) and detailed coil models.

Tachas *et al* (2013) modelled a figure-of-eight coil with different degrees of accuracy to investigate the impact on the induced EF distribution in a realistic head model using an FDM (impedance method). Modelling the figure-of-eight coil using single thin-wire loops yielded inaccurate induced EF distributions. Double thin-wire loops (approximating outer and inner windings of the coil) compared well to multiple-thin wires (spiral-based approach approximating realistic coil winding).

Petrov *et al* (2017) evaluated different models of a figure-of-eight TMS coil with different levels of modelling complexity: single-thin wire loops, multiple thin wires (spiral-based approach), and stacked multiple thin wires that consider the thickness of the winding. There was a significant difference between single-thin and multiple-thin wires approaches. The thickness of the coil winding affected the induced EF minimally. Multiple-thin wires for coil geometry was important to simulate the induced EF accurately and to ensure reliable predictions of neuronal activation.

Nieminen *et al* (2015) introduced an instrument for automated measurement of the E-fields induced by TMS coils in spherically symmetric conductors approximating the head. Later, Çan *et al* (2018) modelled three types of TMS coils using thin-wire approximation for current loops. The calculations and measurements in a spherical phantom showed that the induced EF distribution was highly consistent with the measurements for all coil types.

Gomez *et al* (2020) showed that magnetic coil models constructed from magnetic or current dipoles produced errors smaller than 2% in the primary EF when compared to thick solid-conductor coils. The error could be further reduced by increasing the number of dipoles. Ignoring the eddy currents in the coil windings could generate a maximum point-wise error below 5% of the induced EF in a spherical model.

In summary, the modelling fidelity of the TMS coil was revised in different studies. It was determined that single thin-wire loop representing the coil was inaccurate (Tachas *et al* 2013, Petrov *et al* 2017). If the winding arrangement significantly resemble the experimental coil, the induced EF was consistent with experimental measurements (Çan *et al* 2018). Overall, the methods typically used for modelling magnetic coils can sufficiently suppress numerical errors (Gomez *et al* 2020). Finally, the comparison between

computed and measured induced EFs demonstrated good agreement, suggesting good confidence in the dosimetry techniques (Salinas *et al* 2009, Nieminen *et al* 2015, Çan *et al* 2018).

3.5. Effects of anatomical and inter-individual factors

Adopting realistic head models is a requirement to achieve good accuracy of the computed induced EF when compared to simplified geometries (subsection 3.1). Brain and non-brain tissues present large variability in terms of size and shape among subjects and groups of subjects (e.g. age and gender). Inter-subject variability and specific anatomical aspects affect the induced EF. The extent of inter-individual variability affects how well the findings obtained in one head model can be generalised to a population. Here, we review a total of ten papers accounting for the effects of individual anatomical factors on the induced EF.

Opitz *et al* (2011) showed that the induced EF strength depends on the individual cortical folding pattern using the FEM. The EF strength is selectively enhanced at the gyral crowns and lips, and high EF strength can also occur deep in the white matter. These effects might create hot spots in white matter, resulting in potential neural excitation.

Bijsterbosch *et al* (2012) demonstrated that subject-specific gyral folding patterns and local thickness of subarachnoid CSF are necessary to determine potential stimulation sites accurately using the FEM. Their computation showed that high induced EFs occurred primarily on the crowns of the gyri which had only a thin layer of CSF above them. Consequently, the peak EFs can occur in grey matter regions distant from the assumed spot underneath the centre of the figure-of-eight coil depending on the local variations of CSF thickness. Further, the authors compared two subjects (male and female). The female model had a lower peak intensity (0.6 times lower), partially owing to the larger scalp-cortex distance.

Janssen *et al* (2013) investigated the effect of the sulcus width (<1.5 mm) on the induced EF strength in a head model using the FEM. They determined that the sulcus width did not cause large differences in the majority of the EF strengths. However, considerable overestimation of sulcus width (and consequently thin gyri) produced an overestimation of the calculated EF strength.

Opitz *et al* (2013) generated realistic head models of five subjects and used the FEM to compute the induced EF distribution on the motor cortex. The authors observed that individuals having a hand motor cortex that was shaped like an inverted omega responded preferentially to a 45° coil orientation, while one subject having a hand motor cortex shaped like an epsilon responded preferentially to a 90° coil orientation.

Crowther *et al* (2014) showed a significant difference in the induced EF between four models (adult man, adult woman, girl, and boy). Higher EF strength was observed in younger and smaller brain models.

In Yamamoto *et al* (2016), six individual head models were constructed by segmenting MRI data. The SPFD method was used to compute the induced EF strength at resting motor threshold (RMT) in the motor cortex of each subject. The EF strengths on the target region had a normalised standard deviation of 18% (mean value of 203 V m^{-1}).

Lee *et al* (2016) investigated how the induced EF is affected by brain-scalp distance using heterogeneous head models constructed from MRI data of 50 subjects (with a maximum age of 36 years). With an increment in brain-scalp distance, the maximum EF decreased while the stimulation area increased.

Laakso *et al* (2018) calculated the induced EF strength in 19 subjects using the FEM. The maximum EF strength calculated at active motor threshold (AMT) and RMT had normalised standard deviations of 19% and 15% (mean values of 129 V m^{-1} and 166 V m^{-1}), respectively. The same group (Çan *et al* 2019) extended the analysis to cerebellar TMS for the same subjects. The normalised standard deviations of the maximum EF strength in the cerebellum ranged between 10% to 20%, depending on the type of the magnetic coil and its location.

Gomez-Tames *et al* (2018) determined for each point in the cortex the coil location and orientation that maximized the induced EF strength using the SPFD method. Between 18 subjects, the normalised standard deviation of the maximum EF strength varied from 5% to 40%, with an average of 20%. The variability of the maximum EF strength was minor at the motor or sensory areas where the sulcus was approximately in the same direction in all individuals. The variability was larger in other regions, which had complicated, variable, and distinct folding patterns between individuals.

Zhong *et al* (2019) demonstrated the difference between two coils (conventional figure-of-eight coil and the coil used for deep brain stimulation) targeting the cerebellum in 50 subjects using the FEM. The maximum induced EF strength had a normalised standard deviation ranging from 20%–34% among subjects in the target regions.

In summary, various studies have investigated inter-subject variability of the induced EF ranging from a few to up to 50 subjects (Bijsterbosch *et al* 2012, Crowther *et al* 2014, Lee *et al* 2016, Yamamoto *et al* 2016). There was consensus that the EF strength and hot spot localisation depend on individual anatomical

Table 2. Metrics for transcranial magnetic stimulation coil design and optimisation.

Metric	Quantity	Description	Studies
Depth	EF-decay	EF vs penetration distance in the brain	(Roth *et al* 2002, Kim *et al* 2006, Salvador *et al* 2009, Hernandez-Garcia *et al* 2010, Lu and Ueno 2015a, Lu and Ueno 2015b, Sekino *et al* 2015, Wei *et al* 2017)
	Depth $d_{1/x}$	Depth where EF is larger than E_{max}/x along the line between E_{max} position and the centre of the brain[a, b, c]	(Deng *et al* 2013, Guadagnin *et al* 2016, Gomez *et al* 2018, Gomez-Tames *et al* 2020a)
Focality	Area ($A_{1/x}$)	Cortical area where EF is larger than E_{max}/x	(Im and Lee 2006, Salvador *et al* 2009, Koponen *et al* 2015, Yamamoto *et al* 2015, Rastogi *et al* 2017)
	Volume (V_{Ω})	Mean value of EF over domain Ω	(Hernandez-Garcia *et al* 2010)
	Volume ($V_{1/x}$)	Volume where EF > E_{max}/x	(Guadagnin *et al* 2016, Rastogi *et al* 2017, Samoudi *et al* 2018)
	Volume (V_{th})	Volume where EF > threshold value *th*. Usually normalised by brain volume	(Deng *et al* 2014, Lu and Ueno 2015a, Lu and Ueno 2017, Wei *et al* 2017, Gomez *et al* 2018)
	Spread ($S_{1/x}$)	$S_{1/x} = V_{1/x}/d_{1/x}$	(Deng *et al* 2013, Gomez *et al* 2018, Gomez-Tames *et al* 2020a)
Energy	Coil energy	Minimum coil magnetic field energy	(Koponen *et al* 2017, Wang *et al* 2018b)

[a] E_{max} is usually at the cortex.
[b] Variable x is usually 2 or $\sqrt{2}$.
[c] Centre of the brain was considered under Cz at a height of T3 and T4 (10–20 EEG system) in anatomical head model or centre of spherical head model.

differences (Opitz *et al* 2011, Bijsterbosch *et al* 2012, Janssen *et al* 2013). Also, the EF variability may be different according to the targeted brain part and population segment (Bijsterbosch *et al* 2012, Lee *et al* 2016, Gomez-Tames *et al* 2018, Zhong *et al* 2019). In the studies reviewed in this and other subsections, adults have been the predominant population segment (figure 5(b)), and the elderly and youth populations are almost unexplored. Further, TMS targeting the prefrontal and motor-sensory areas accounted for 74% of the studies, followed by deep and cerebellar areas (16%). Parietal, temporal, and occipital accounted for 10% of the studies, as illustrated in figure 5(c).

3.6. Coil design: optimisation and performance

The circular coil was the first design used for TMS in the seminal work presented in (Barker *et al* 1985). The first successful attempt to optimise the TMS coil for better focality used the figure-of-eight coil, which was presented by Ueno *et al* (1988). Here, we identified 23 studies that have used EF calculations to investigate coil design, optimization, and performance. As listed in table 2, the studies have used various metrics, such as depth and spread of the induced EF or energy requirements, to optimise and study the performance of various coil designs.

Roth *et al* (2002) proposed the first coil designed for the stimulation of deep brain regions termed Hesed coil (H-coil). The H-coil demonstrates a slower decrease of the induced EF as a function of the distance from the coil centre than that in double cone and circular coils. This was confirmed by phantom measurements and numerical computation.

To reduce the spread of the induced EF and improve focality, Kim *et al* (2006) computed the effect of passive shielding plates that partially blocked the electric and magnetic fields. One disadvantage of this method was a reduction in the maximum EF when using the shield plate. A reduction of 50% in the maximum EF strength was observed at a distance of 40 mm from the coil.

Im and Lee (2006) evaluated a multi-coil TMS system using realistic simulations up to 128 small coils. Using this system, enhanced targeting accuracy and concentrated induced EF distribution was possible.

Lu *et al* (2009) presented a multi-coil TMS system with 40 small coils. The induced current density and EF in a realistic human head model were calculated using the FDM. Proper adjustment of the input current phases can improve the induced EF strength in the brain, although coil size does not allow strong fields, such as in the figure-of-eight coil.

Salvador *et al* (2009) showed that a high permeability core in an H-coil could increase focality and field intensity by 25%. The performance of the proposed design was investigated using a realistically shaped homogeneous head model.

Hernandez-Garcia *et al* (2010) considered shielding of the TMS coil by using a secondary coil, which created opposing electric and magnetic fields that cancelled the field of the source outside the region of

interest. Iterative optimisation techniques were used to design shields for the figure-of-eight coil by considering two objectives: selectivity and depth of the primary EF computation for a spherical model. The resulting designs were tested on a realistic human head model. For the same penetration depth the volume was reduced by 13% for the shielded case relative to the unshielded case.

Deng *et al* (2013) quantified the spread and depth of the induced EF to characterise the performance of 50 TMS coils using a spherical model. For any coil design, the ability to directly stimulate deeper brain structures was obtained at the expense of inducing a wider electrical field spread; moreover, none of the coil designs was able to overcome the depth–focality trade-off. However, the figure-of-eight-shaped coils were more focal (the area where the field strength becomes half of the maximum; 5 cm^2) when compared to circular coils (34 cm^2).

Deng *et al* (2014) showed that larger coils were more appropriate for deep TMS by analysing the depth–focality trade-off of the EF in a spherical head model. Coils with larger diameters had an EF that decays slower in depth but was less focal than that of smaller diameters. Although smaller coils had superior focality than the larger coil, the advantage in terms of activated brain volume diminished with increasing target depth. The double cone coil offers high energy efficiency and balance between stimulated volume and superficial field strength. Although, TMS targets at depths of approximately 4 cm or more results in superficial stimulation strength that may compromise upper limits in TMS safety.

Sekino *et al* (2015) developed an eccentric figure-of-eight coil that reduced the coil driving current by 20% when compared to the conventional figure-of-eight coil while still inducing similar EF strength.

Koponen *et al* (2015) introduced a method to determine the minimum-energy solution for a TMS coil using a spherically symmetric head model for optimisation with given focality constraints. The optimised coil design demonstrated a 73% reduction in power requirement when compared to the figure-of-eight coil with similar focality.

Lu and Ueno (2015b) investigated the conventional figure-of-eight coil working with the Halo coil (i.e. Halo–figure-of-eight assembly (HFA) coil), which was computationally analysed for deep TMS in anatomical head model. The HFA coil improved the penetration depth of the magnetic field more than the figure-of-eight coil. In a subsequent work by the same group (Lu and Ueno 2015a), a figure-of-eight coil working with the circular coil (Halo–circular assembly (HCA) coil) showed an increase at the expense of reduced focality. Further, Lu and Ueno (2017) extended the comparison by including H- and double cone coils. The simulation results demonstrated that double cone, H-, and HCA coils had deeper penetration depth than in the conventional figure-of-eight coil, at the expense of higher and wider spread of induced EF in superficial cortical regions.

Yamamoto *et al* (2015) proposed a bowl-shaped coil that induces EFs in a wider area of the brain than a figure-of-eight coil. The electromagnetic characteristics of the coil were analysed. A more uniform induced EF can reduce the burden of coil-positioning error but at the cost of focality.

Guadagnin *et al* (2016) conducted a comparison of 16 different coils (figure-of-eight, large circular, H1-, double cone coils) for deep TMS. The EF distributions were calculated in several brain structures of a head model. The results showed that only the coils of the double cone family were able to reach the distance of deep brain regions (>4 cm from the cortex); however, this method demonstrated lower focality.

Rastogi *et al* (2017) proposed a quadruple butterfly coil (QBC) with a high permeability ferromagnetic material acting as a passive magnetic shield of semi-circular shape. The QBC with a shield was compared with a QBC without a shield and the figure-of-eight coil in 50 anatomically realistic heterogeneous head models targeting two brain regions: the vertex and the dorsolateral prefrontal cortex. The shielding solutions showed an improvement in focality of 20% when compared to the conventional figure-of-eight coil and 12% when compared to QBC alone.

Wei *et al* (2017) investigated multi-coil array optimisation by investigating induced EF in a spherical head model. Marginal improvement was observed for the multi-coil arrays when compared to the figure-of-eight coil in terms of the half-depth distance.

Koponen *et al* (2017) developed a TMS coil optimisation method in a realistic head geometry with an arbitrary overall coil shape to increase the energy efficiency for focal stimulation. They used the BEM with three-layer head models for computing the induced EF on the cerebral cortex. The optimized coil resulted in an eccentric figure-8 coil with centre-dense winding. The optimisation could increase TMS coil efficiency by a factor of two compared to the standard figure-of-eight coil.

Iwahashi *et al* (2017) proposed a method to evaluate the average coil performance for a group of individuals. To demonstrate the effectiveness, 10 head models comprised of 10 tissues were used. The results showed that there was no remarkable difference between six coils (figure-of-eight coils with and without shielding, eccentric figure-of-eight-type coils) for selectively inducing the maximum EF within the region of interest, although the focality could be improved by considering metallic plates (passive shielding).

Samoudi *et al* (2018) proposed the double cone coil with the Halo coil (i.e. Halo–double cone assembly (HDA)) and compared it with the HFA, double cone, and Halo coils. Computational analysis of the induced EFs reaching the hippocampus, nucleus accumbens, and cerebellum in a realistic head model showed that only the HDA coil reached the hippocampus and nucleus accumbens with an EF larger than 50% of the maximum value in the cerebral cortex.

Gomez *et al* (2018) presented a methodology for optimisation of TMS coils. A multi-objective optimisation technique was used for computationally designing TMS coils that achieved optimal trade-offs between EF focality in spherical and MRI-derived head models. The proposed minimum-energy coil resembled eccentric double cone coil with centre-dense winding.

Wang *et al* (2018b) presented a pipeline to produce coil windings conformed to a spherical surface that can reliably replicate the induced EF distribution on the cortex generated by existing TMS coils while significantly improving energy efficiency. Simulations in a realistic head model demonstrated that the EF induced by the proposed coil (eccentric double cone coil with centre-dense winding) matched that induced by the original coil in both superficial and deep brain regions.

Gomez-Tames *et al* (2020a) compared TMS coil designs for targeting deep brain regions for 18 subjects. For optimised coil positioning to target deep brain regions, the highest EF generated in deep brain regions was 50% of the maximum value in the cortex for the HCA. The systematic analysis also confirmed the trade-off between spread and penetration, where the double cone type coil demonstrated the best performance.

In summary, computational modelling studies were conducted to improve focality, depth, and power requirements, as listed in table 2. In general, smaller coils have superior focality but lower depth (Thielscher and Kammer 2004, Deng *et al* 2013, Sekino *et al* 2015), while larger coils favour deeper targets (Roth *et al* 2002, Deng *et al* 2014, Lu and Ueno 2017, Samoudi *et al* 2018). Nevertheless, all coils are subject to a trade-off between depth and focality (Deng *et al* 2014, Guadagnin *et al* 2016, Gomez *et al* 2018, Gomez-Tames *et al* 2020a). Shielding approaches may increase the focality at the expense of a reduction in the maximum EF (Kim *et al* 2006, Hernandez-Garcia *et al* 2010, Iwahashi *et al* 2017); further, multi-coils have been investigated to improve focality; however, no significant improvement with respect to the figure-of-eight coil was achieved and the method demonstrated difficulty in practical implementation (Kim *et al* 2006, Lu *et al* 2009, Wei *et al* 2017). Among standard commercial coils for deep TMS, the double cone coil offers a balance between stimulated volume and superficial field strength (Deng *et al* 2014, Guadagnin *et al* 2016, Gomez-Tames *et al* 2020a). Multi-objective optimisation of the coil windings can reduce the required power and reach the physical limits of the trade-off between depth and spread (Hernandez-Garcia *et al* 2010, Koponen *et al* 2015, 2017, Gomez *et al* 2018, Wang *et al* 2018b). There was agreement that eccentric coil windings (centre-dense) provide the optimal geometry for minimum-energy requirements (Koponen *et al* 2017, Gomez *et al* 2018). The spherical head model provides a standardised platform to evaluate and compare coil designs but with limitations (refer subsection 3.1). Conversely, systematic evaluation of the coil performance in a group of anatomically realistic head models may present more robust analysis (Iwahashi *et al* 2017, Rastogi *et al* 2017, Gomez-Tames *et al* 2020a).

3.7. Guiding TMS dose

There are no easily measurable responses for the activation of cortical areas other than the areas related to motor/language/visual functions. An initial approach was to use the excitation threshold measured in the motor cortex to estimate the cortical excitability at other cortical sites. In this subsection, six studies have been identified that used computational dosimetry to simplify the selection of stimulation parameters.

Stokes *et al* (2013) used a realistic head model to show that the coil-cortex distance was approximately linearly proportional to the EF induced in the cortex. They proposed the utilisation of the coil-cortex distance as a correction factor to adjust the TMS intensity for other cortical areas based on the measurements in the motor and visual cortices. Two weaknesses were demonstrated, i.e. the intra-individual differences in cortical targets and the effect of coil orientation, which have a large influence on the stimulation efficiency.

Janssen *et al* (2014) utilised EF calculations in a realistic head model and showed that a simple correction based on the inverse of the coil-cortex distance does not adjust the induced EF for regions other than the motor cortex.

Janssen and Oostendorp (2015) examined the induced EF for different coil orientations in 14 cortical targets of one head model (eight tissues). The EF perpendicular to the anterior sulcal wall of the central sulcus was highly susceptible to coil orientations and had to be adjusted for maximising the EF in the motor cortex. Small orientation changes (10°) did not alter the induced EF drastically. Orienting the TMS coil based on anatomical information (MRI) about the targeted brain area can improve the EF, though those orientations determined in one model may be suboptimal for other individuals.

Opitz *et al* (2016) proposed a TMS guiding method by targeting the EF in specific brain regions associated with functional network maps based on resting-state functional MRI (fMRI). A simulated atlas of regions with low coil orientation-sensitivity can be provided in the absence of TMS dosimetry and fMRI data to personalise coil parameters.

Gomez-Tames *et al* (2018) developed an atlas to guide the coil orientation and position to group-level optimisation using 18 head models. A universal optimal coil orientation applicable to most subjects was feasible at the primary somatosensory cortex and primary motor cortex. The optimal coil orientation corresponded to an induced EF direction perpendicular to the sulcus wall following the anatomical shape of the hand motor area. Individualised computation of the induced EF became more important in other cortical regions, which had higher inter-subject variability of the cortical folding.

Li *et al* (2019) used an optimisation technique to reduce the number of computations to determine the optimal TMS coil configuration to target specific brain regions. Up to 11 iterations of EF computations were required for high accuracy in 13 head models under this test.

In summary, the computation of the induced EF to guide TMS (position and orientation) becomes more relevant owing to a lack of easily measurable responses in most of the cortical regions. Moreover, TMS-induced EF is sensitive to coil orientation that does not allow the application of simplified methods using coil-scalp distance or even simplified head models to estimate the induced EF (Janssen and Oostendorp 2015). Thus, computation using individualised head models together with TMS coil navigation is the most accurate method to determine the induced EF. Alternatively, a group-level analysis of the induced EF is proposed to guide TMS using an TMS atlas that is optimized for a population (Gomez-Tames *et al* 2020a).

3.8. TMS localisation and validation

During the application of TMS, the site and size of the stimulated cortical volume are unknown. EF dosimetry combined with electrophysiological measurements can be used to gain insight on the activated neural structures in the brain and to validate the EF models. In this subsection, we identified 11 studies that investigated EF-based metrics for TMS localisation and compared and validated with electrophysiology measurements and direct electrical stimulation (DES) on the cerebral cortex.

3.8.1. Comparison with electrophysiology measurements.

Thielscher and Kammer (2002) reported the first combination of physiological measurements with induced EF modelling. Based on measured threshold stimulator intensities in four subjects, the field distribution on the individual cortical surface was calculated using a spherical head model. The authors proposed the most likely stimulation point at which the variance of the induced EF strengths over all stimulation sites was minimal (lateral part of the hand knob, which is an anatomical region of the hand motor cortex).

Opitz *et al* (2013) measured the MEP during TMS targeting the right first dorsal interosseous (FDI) muscle and modelled the induced EF in four subjects. The MEP was measured using two different coil orientations (45° and 90° to the midline) at 25 different locations (5 × 5 grid, 1 cm spacing) over the left motor cortex. There were strong correlations for the regression between MEP amplitudes and the calculated mean EF induced in the M1 ($0.70 < r < 0.91$, $n = 4$). Furthermore, the locations of the highest EF strengths were consistent with blood oxygen level-dependent fMRI measurements while subjects voluntarily moved their right index finger.

Krieg *et al* (2015) investigated the relationship between induced EFs and cortical activation measured indirectly through functional imaging concurrent with TMS. They observed that decomposing the EF into orthogonal vector components based on the cortical surface geometry (and hence, cortical neuron directions) resulted in significant differences between the regions of the cortex that were active and non-active. Later, Arabkheradmand *et al* (2019) developed an algorithm based on EF calculations and functional neuronal models for predicting the physiological responses evoked by TMS.

Bungert *et al* (2017) used MRI-based head models for individualised estimation of the EF induced in nine subjects. The motor thresholds in the FDI and abductor digiti minimi muscles were measured in the same subjects. The authors compared the normal component and strength of the EF with the variations in the measured motor thresholds of two muscles when the coil was rotated. They observed that the EF strength on the crown of the precentral gyrus was significantly related to the measured motor threshold, which indicated that TMS activated a focal region around the gyral crown.

Laakso *et al* (2018) modelled the motor cortical TMS in MRI-based models of 19 individuals. The AMT and RMT of the FDI muscle were measured at 3 to 5 coil locations. The authors showed that the induced EF in a small region in the hand knob of M1 was significantly related to the measured MTs. At the group-level, the EF in the ventral and lateral part of the hand knob demonstrated approximately 70% variability in the MT owing to coil location.

Mikkonen *et al* (2018) measured the RMT in the FDI muscle and calculated the induced EF in 28 subjects. The individually calculated mean EF strength in the motor cortex significantly correlated with the measured RMT ($R^2 = 0.44$).

Weise *et al* (2020) performed motor-cortical-based TMS measurements using several coil locations and orientations in 15 subjects and modelled the induced EFs using MRI-based head models. By investigating the congruence of the calculated EF and the measured MEP amplitudes, the authors showed that the origin of MEPs was around the gyral crowns and upper parts of the sulcal wall, and that the EF strength was the most relevant quantity to explain the observed effects. For validation, the authors optimised the position and orientation of the TMS coil to produce the maximum EF strength at the identified cortical location. The optimised scenario showed a reduction of the TMS intensity to generate similar MEPs, thereby validating the computational model.

Reijonen *et al* (2020) measured the RMT of the FDI muscle and modelled the induced EF in 10 subjects. The relationship between the calculated EF strength and the measured RMT suggested that the activation site of TMS was focal and located in the hand knob area of the motor cortex.

Studies on the relationship between the EF and measured electrophysiological response (hand motor response) have been conducted to determine the activation site in the brain. The studies agree on identifying a significantly localised activation site in the somatotopically organised motor cortex (Krieg *et al* 2015, Bungert *et al* 2017, Laakso *et al* 2018, Weise *et al* 2020). However, there is no consensus on the best EF-based metrics (e.g. EF strength or the normal or tangential EF component) or the specific gyral activation site (i.e. crown or upper parts of sulcal wall).

3.8.2. Comparison with direct electric stimulation (DES).

Opitz *et al* (2014) compared the computationally predicted stimulation area in TMS with the DES in six patients with tumours near precentral regions. The authors used an MEP mapping experiment combined with realistic individual simulations of the EF distribution during TMS. The stimulation areas in TMS and DES showed an overlap of up to 80%. The Euclidean distance between the centre of gravity of the TMS map and that of the DES map was 6 mm and 9 mm, respectively.

Aonuma *et al* (2018) proposed a post-processing method to determine TMS activation sites by combining the individualised computed EFs for the coil orientations and positions that delivered high MEPs during peritumoral mapping. Peritumoral mapping by TMS was conducted on patients who had intra-axial brain neoplasms located within or close to the motor speech area. The hand motor areas estimated by this proposal and DES were in good agreement (5 mm distance error) in the ipsilateral hemisphere of four glioma patients. The hotspots predicted by the method used by the authors were better than those identified by a navigation system that is based on spherical model computations.

Seynaeve *et al* (2019) investigated preoperative mapping based on TMS-induced EF computation in 12 patients. By comparing with DES, the authors argued that the weighted average of the induced EFs calculated with a realistic head model demonstrated superior performance in comparison with other metrics (nearest or perpendicular projection from the coil and location of maximum EF strength). The Euclidean distance between TMS estimation and DES mapping was 11 mm.

Comparison with DES showed that functional localization was possible with a prediction error in the order of 5 to 11 mm by TMS dosimetry. One caveat for the comparison between DES and TMS is that the two methods differ in terms of the EF direction. In the former, the EF is radial from the electrode, whereas the latter is not limited to the direction that is normal to the cortical surface. Thus, TMS may activate different circuits within the same gyrus, considering that the motor system is topographically organised.

4. Models of neural activation

Experimental studies have been fundamental in identifying mechanisms that could explain neural responses to magnetic stimulation. However, they predominantly used indirect and non-invasive measurements, such as brain imaging and biomarkers of physiological responses (i.e. neuromuscular, speech arrest, phosphene). Directly monitoring the neuronal response during magnetic stimulation would facilitate the understanding of the effects of TMS; however, only a few *in-vitro* studies exist. Conversely, *in silico* studies of neuronal activation can provide new insights at a cellular level and optimise stimulation parameters that cannot be achieved by *in-vitro* approaches and imaging modalities. We have identified and reviewed 18 papers that have used biophysical-based neuron models for studying the mechanisms of TMS at micro-scale, while meso-scale modelling of brain networks was beyond the scope of the present review and interested readers may wish to consult (Esser *et al* 2009). A summary of the papers is listed in table 3, and a detailed review of the studies is given in the following subsections.

Table 3. Multiscale studies for magnetic exposure on central nervous system.

Study	Neural morphology[a]	Neuronal elements[b]	Activation site	Head model[c]	Others
Nagarajan *et al* (1993)	Simple	Small axon, GC	Terminals	×	×
Nagarajan and Durand (1996)	Simple	Myelinated axon	N.A	×	×
Hyodo and Ueno (1996)	Simple	Myelinated axon	Terminals/bending	×	×
Nagarajan *et al* (1997)	Simple	Myelinated axon	Terminals/along axon	×	×
Kamitani *et al* (2001)	Realistic	Layer 3 (L3) PN	Dendrites	×	×
Pashut *et al* (2011)	Realistic	L3 PN	Soma	×	×
Salvador *et al* (2011)	Realistic	L5 PN, IN, AF	○Fiber bends (PN track) ○Axonal terminations (interneurons and collaterals) ○Combination (association fibers)	◯	×
De Geeter *et al* (2015)	Simple	PNT, AF	Stimulation tract's position according to TMS coil orientation	◯	DTI
Goodwin and Butson (2015)	Realistic	L3 PN	Initiation at neural elements (dendrite, soma, axon) depends on the coil orientation	◯	×
Wu *et al* (2016)	Realistic	PN, IN.	Competition of various neuronal elements. Determined by the local geometry and field orientation/waveform	×	×
De Geeter *et al* (2016)	Realistic	PN	No discussed	◯	DTI Navigation system
Seo *et al* (2017)	Realistic	L3 and L5 PNs	Mostly at axon initial segment and a few near boundary GM/WM	◯	×
Moezzi *et al* (2018)	Complex	IN synapse onto L5 PN that synapse onto motor neurons	No discussed	×	×
Wang *et al* (2018a).	Simple	Myelinated axon	Axonal undulation can affect thresholds	×	×
Soldati *et al* (2018)	Simple	PNT	Axonal termination in gyrus/lip of crown	◯	Navigation system
Aberra *et al* (2020)	Realistic	L1 to L4 including Neurogliaform, PN, large basket	Mixed	◯	×
Gomez-Tames *et al* (2019, 2020b)	Simple	PNT	Bends for PN tract	◯	◯

[a]Simple refers to a neuron without bifurcations.

[b]PN: pyramidal neuron; PNT: pyramidal neuron track; IN: cortical interneuron; GC: granule cell; AF: associate fibres; AC: axonal collaterals.

[c]◯: head models with at least five tissues (scalp/skin, skull, CSF, grey matter, and white matter) with realistic cortical folding representation; △: includes gyral/sulcus structure; ×: otherwise.

4.1. Multi-compartment conductance-based model approach

Early modelling studies provided mathematical formalism of polarisation and activation of simplified neuronal structures. They used infinite cables in length representing unmyelinated and myelinated axons that are required to understand the effects of magnetic stimulation at the level of the peripheral nervous

system (Reilly 1989, Roth and Basser 1990). In this subsection, simple models for investigating the coupling with TMS-induced EF are revised.

To apply earlier neuronal models to the CNS, Nagarajan *et al* (1993) focused on the magnetic stimulation of short-length neuronal structures, in which the activation at axon terminals follows the EF instead of its gradient, such as in long structures. Thereafter, Nagarajan and Durand (1996) also clarified that both primary and secondary field components (not just the primary component) contributed to excitation and provided a generalised cable equation to account explicitly for both components. At the same time, the validity of this generalised 1D cable equation for magnetic stimulation was shown to be valid not only for isolated axons but also for the axons in nerve bundles.

In Kamitani *et al* (2001), the authors coupled the external field by transforming the induced EF into an equivalent intracellular current that was injected into each segment of the cable. The authors also described methods to deal with the injected current in branching and at the terminals of neural structures that allowed the analysis of multi-compartmental realistic neocortical neurons. A similar approach can be observed in (Wu *et al* 2016).

Wang *et al* (2018a) investigated and added mathematical rigour to the validity and implications of the method presented in Nagarajan and Durand (1996) to present an alternative coupling approach, termed quasi-potential method, which was applied in other study as well (Goodwin and Butson 2015). The quasi-potential method essentially allows coupling of the EF induced by magnetic stimulation to neuronal membranes by integrating the longitudinally induced EF along with the branching structure of the neural cable model, as presented in equation (5).

4.2. Level of morphological representation

Neurons in the motor cortex present different susceptibilities to the induced EF, which varies according to location of the neuronal elements and their relative orientation to the induced EF, as well as intensity and waveform of the induced EF (Lazzaro *et al* 2001, Di Lazzaro *et al* 2004). In this subsection, studies that have used neuronal models to investigate the mechanisms of TMS in the motor cortex have been reviewed.

In the study presented by Hyodo and Ueno (1996), the computational simulation suggested that the termination points of nerves or the bent part of an axon are low threshold stimulation sites when magnetically stimulated with a figure-of-eight coil. Further, Nagarajan *et al* (1997) observed similar results when investigating excitation sites for different positions of a round and butterfly coil during *in-vitro* magnetic stimulation.

Kamitani *et al* (2001) investigated the effects of the induced EF in a realistic multi-compartmental model of a layer 5 pyramidal cell model. The magnetic stimulation acted on the dendrites in neocortical neurons. The simulation showed brief burst firing followed by a silent period of duration, which is comparable to the experimental data of single-pulse TMS. Further, the simulation showed that the neurons were readily activated to TMS under background synaptic inputs in agreement with experimental results that showed that TMS effects are evoked with lower intensity during muscle contraction.

Pashut *et al* (2011) investigated the complex representation of CNS neurons. They argued that the magnetic stimulation of CNS neurons depolarised the soma, leading to the initiation of an action potential in the initial segment of the axon. Here, passive dendrites affected this process primarily as current sinks, not sources. However, the possible inaccurate implementation in the current injection method was speculated in other work that could change the estimated origin of activation (Wang *et al* 2018a).

Wu *et al* (2016) implemented a multitude of detailed physiological and morphological properties of pyramidal cells. The activation thresholds and sites were computed to various field directions and pulse waveforms. The dependence of the initiation sites on both the orientation and the duration of the stimulus implies that the cellular excitability might represent the result of the competition between various firing-capable axonal components.

Moezzi *et al* (2018) proposed a biophysical model of electromyography (EMG) signal generation based on the feed-forward CNS network coupled with a pool of motoneurons. The simulated EMG signals matched experimental EMG recordings in shape and size.

4.3. Multiscale models and applications using induced EF in realistic head models

In addition to neural modelling, small geometrical alterations, tissue heterogeneity, and tissue conductivity can alter the field distribution and therefore affect the site of activation (refer subsections 3.1 and 3.3). The path of the nerve fibres, which can be determined using tractography, also affects the patterns of activation (Opitz *et al* 2011, Nummenmaa *et al* 2014). This subsection reviews studies that considered realistic neuron models driven by TMS-induced EFs that were computed in a realistic human head model.

Salvador *et al* (2011) investigated neuronal responses using a simplified cortical sulcus model for TMS with various structures, including pyramidal neurons, interneurons, and association fibres embedded in the

grey matter and projecting to white matter, which were considered to be the cause of the generation of evoked motor responses. They identified changes in the stimulation threshold that could be shaped by field orientation (coil orientation), pulse waveform, and diameter of neurons. The outcome was that TMS preferentially activated different sets of axons depending on their orientation with respect to the induced current. For instance, neurons modelling pyramidal neuron tracts were excited in the white matter where they were bent. Conversely, cortical interneurons and axon collaterals were excited at their axonal terminations. Finally, pyramidal association fibres were stimulated either at their axonal termination or at a sharp axonal bend.

Goodwin and Butson (2015) integrated anatomically realistic head models derived from MRI data and detailed models of pyramidal cells. This work allowed the visualisation of activated axons of pyramidal cells within a patch of cortex on a subject-specific basis.

De Geeter *et al* (2015) used personalised anisotropic head model tissues with realistic neural trajectories of the subject, obtained from tractography, based on diffusion tensor images. An investigation of the impact of tissue anisotropy showed that its contribution was not negligible. In contrast, the model proved to be less sensitive to the uncertainty of the tissue conductivity values.

De Geeter *et al* (2016) used an anisotropic head model with white matter fibre tracts obtained from the patient. The computed induced EF corresponded to different coil positions during the speech arrest experiment, in which TMS was delivered to Broca's area. The authors computationally determined the tract that was activated when a speech arrest occurred.

Seo *et al* (2017) incorporated layer 3 and layer 5 pyramidal neurons into realistic head models that considered the intricate folding patterns of the cortex. They observed that the action potentials were predominantly generated at the initial segment of the axon.

Soldati *et al* (2018) used individualised MRI-based computer simulations for the determination of brain stimulation thresholds. The computed EFs were based on the same TMS parameters (TMS coil design and its position and orientation) during measurements that produce muscle responses at threshold intensity. Statistical analyses were performed to evaluate the minimum EF intensities needed for exciting the motor cortex. These values were used to estimate parameters in established biological axon models. The combined approach with established biological axon models enabled the extrapolation of the measured thresholds for sinusoidally varying EFs to be compared with present human safety guidelines for human protection against electromagnetic exposure.

Gomez-Tames *et al* (2019) investigated stimulation thresholds computing the effects in pyramidal tracts embedded in the cortical folding by independent implementations of neural and induced EF computations. Moreover, Gomez-Tames *et al* (2020b) computed experimentally-derived EFs to determine the activation of the pyramidal tract model embedded in the head models to derive the activation site on the cortical surface at the macroscopic level. The stimulation site was determined in the upper part of the gyrus for suprathreshold stimulation for relaxed muscles. Also, a good correlation between experimental and multiscale-derived thresholds was achieved ($R^2 = 0.6$).

Aberra *et al* (2020) used a variety of realistic models of neurons across the cortical layers to quantify the effect of TMS with several combinations of pulse waveforms and current directions on the activation of individual neurons. The intracortical axonal terminations in the superficial gyral crown and lip regions were activated with the lowest TMS intensity. The neural activation was primarily driven by the field strength, rather than the field component that was normal to the cortical surface. Changing the induced current direction caused a shift in the activation site, which may explain the differences in thresholds and latencies of muscle responses observed in experiments.

4.4. Summary

As listed in table 3, there is a trend of increasing complexity in the morphology of the neuron modelling that is used to investigate the activation thresholds of individual neurons. Also, neuronal model embedded in realistic head models permits the computation of neuronal activation using individualised EFs. Further, recent studies have developed network models that may explain the generation of different evoked responses. These approaches show the possibility of combining experimental TMS parameters (coil design, position, and orientation) with subject-specific modelling to quantify the excitation of cortical neurons.

The mentioned multiscale approaches may be applied in improving the specificity of preoperative mapping of brain functions in neurosurgery (De Geeter *et al* 2016). Also, knowledge of the TMS mechanisms at cellular levels can help for clinical diagnosis of electrophysiological responses (Moezzi *et al* 2018, Aberra *et al* 2020). Moreover, multiscale modelling can provide additional scientific rationale to developed safety limits for electromagnetic exposure protection in safety guidelines/standards (Soldati *et al* 2018, Gomez-Tames *et al* 2019, IEEE Std C95.1-2019 2019, International Commission on Non-Ionizing Radiation Protection 2020).

5. Conclusions

TMS is used in the treatment and diagnosis of neurological diseases or conditions, neurosurgery mapping, and as a marker to investigate brain functions. Computational dosimetry techniques have aided in improving the understanding of the TMS-induced EF and how it is affected by anatomical and biophysical parameters. In particular, this review showed that there is a high consensus on the importance of accurate modelling of the complex cortical folding and surrounding CSF for obtaining accurate prediction of the stimulation site.

EF modelling has matured to a point so that individual anatomic models can be efficiently generated from MRI data using modelling pipelines, which allows the construction of an individual model of each participant in experimental studies. Various computational methods can be used for computing the induced EF in anatomical models. Recent studies have shown that all commonly used computational techniques can provide sufficient numerical accuracy for EF calculations (Saturnino *et al* 2019, Gomez *et al* 2020, Soldati and Laakso 2020).

EF dosimetry has been extensively applied for the development of magnetic coils to, e.g. improve the focality of the induced EF while reducing the energy consumption. Despite the inability to model the effects of individual anatomy on the induced EF, simpler spherical EF models are sufficient for the optimisation and characterisation of magnetic coils (Deng *et al* 2013). Computation cannot overcome physical limitations, such as the depth focality trade-off that makes it difficult to design coils to target deep brain areas (Deng *et al* 2013, Gomez *et al* 2018, Gomez-Tames *et al* 2020a). Clinical effects of TMS on deep brain regions are still open for consideration given that presence of high EF on superficial regions and potential distal or indirect effects of stimulation via pathways between superficial and deeper regions that can be explored by dosimetry analysis.

The second application of EF modelling is to guide the selection of TMS parameters for stimulating brain areas that do not produce directly measurable responses. Studies using subject-specific anatomical models have shown that stimulation can be optimised individually or in a group of subjects (Opitz *et al* 2016, Gomez-Tames *et al* 2018, Li *et al* 2019). In future, this may allow personalised stimulation protocols for rehabilitation or therapy. However, these approaches have not yet been tested experimentally.

Analysing the relationship between the EF and electrophysiological data can reveal the sites activated by TMS. Recent studies have focused on the hand area of the motor cortex and have revealed strong correspondence between individually calculated EF strength and measured muscle responses (Opitz *et al* 2013, Bungert *et al* 2017, Laakso *et al* 2018, Weise *et al* 2020, Gomez-Tames *et al* 2020b). The results allow the determination of the site of activation in the motor cortex; this far, studies suggest that muscle responses evoked by TMS originate from a focal area near the crown of the precentral gyrus. Accurately localising the activation sites is relevant, for instance, in preoperative mapping for planning tumour resection. Most of the studies have been focused on the hand motor area. Exploring the relationship of the EF in different areas with not only motor responses but also with linguistic or cognitive tasks can be possible via concurrent imaging studies and dosimetry advances in near future.

In addition to the above-mentioned relationship between the EF and electrophysiological responses, the validity of EF dosimetry models is supported by EF measurements in experimental phantoms (e.g. Salinas *et al* 2009, Nieminen *et al* 2015) and comparison with direct electrical stimulation (Opitz *et al* 2014, Aonuma *et al* 2018, Seynaeve *et al* 2019) or neuroimaging (Opitz *et al* 2013, Ottenhausen *et al* 2015, Arabkheradmand *et al* 2019). Validation and verification of the computed induced EF using *in-vivo* and *ex-vivo* measurements in humans can help to tuned further biophysical parameters to have more accurate predictions (Tischler *et al* 2011, Mueller *et al* 2014, Li *et al* 2017, Opitz *et al* 2017, Vöröslakos *et al* 2018).

Combining EF dosimetry with neuron models, i.e. multiscale modelling, can provide a deeper understanding of the neural mechanisms of TMS. State-of-art models can consider morphologically realistic neuron models embedded in individualised head models (Goodwin and Butson 2015, Seo *et al* 2017, Aberra *et al* 2020). For instance, multiscale models can reveal the types and locations of activated neurons, and they can also be used to study the effects of pulse waveform and EF direction. While such models can explain many characteristics of evoked responses, the model predictions have not yet been fully validated in experiments. Future studies that can combine multiscale models and experimentally measured responses are needed.

Despite many research uses, EF dosimetry in realistic models is not yet a part of clinical workflow. Recent technological progress has been made towards using EF dosimetry in clinical applications. Progress has been made in automatic generation of head models from MRI data (Rashed *et al* 2019, 2020b, Sendra-Balcells *et al* 2020) and approaches for computation of EF in real time have been developed (Laakso and Hirata 2012, Stenroos and Koponen 2019, Yokota *et al* 2019). These advances can allow integration of EF dosimetry as a part of existing neuronavigation systems, which currently employ spherical models for EF estimation. The added value for clinical applications would come from improved accuracy of neuronavigation, e.g. for

preoperative planning. Also, stimulation atlas can be derived for specific populations when time- and cost-constraints exist in resources in small clinics and even hospitals due to operation time limitations.

Future research using multiscale modelling can provide a better understanding of the types and locations of activated neurons, which can potentially enable new TMS-based biomarkers for neurological diseases. Further, this could lead to new ways to optimise stimulation to activate a desired set of neurons, which could improve the value of TMS in treatment and rehabilitation.

Acknowledgments

This work was supported by JSPS Grant-in-Aid for Scientific Research (Grant No. 17H00869 and Grant No. 19K20668) from the Japanese Society for the Promotion of Science (JSPS) and Grant No. 325326 from Academy of Finland Japanese Society.

Appendix A Search strategy

A search strategy was developed to retrieved papers for each subsection of section 3. Another search strategy was developed for section 4. The search database was Web of Science covering the time period from 1990 to 10.02.2020. Google scholar engine was used for identifying studies from 2020 that have not been indexed yet in Web of Science. The detail of the search strategy is presented in table a1.

Table A1. Search strategy used to retrieve papers for the different subsections covering time period: 1990–10.02.2020. The term 'relevant' indicates the number of studies identified from database that were not excluded. The term 'included' refers to the total number of studies included in the corresponding subsection after adding papers identified from other sources.

3.1. Representation of head tissues						
Search data	TI = (TMS OR rTMS OR (Transcranial OR brain) Magnetic Stimulation) AND TS = ('Electric Field$' OR 'Volume Conductor$' OR 'induced current density') AND TS = (('Head$' OR Anatomic* OR Brain OR Cortical OR Spher*) NEAR/5 (Comput* OR Model* OR Simulation$ OR Biophysical)) AND TS = (primary field OR secondary field OR displacement current$ OR boundar* $ OR Inhomogene* OR heterogeneit*)					
Identified from database	38	Excluded (not relevant)	31	Identified from other sources	0	Relevant 7
Included in analysis	7					
3.2 Electrical conductivity: variability						
Search data	TI = (TMS OR rTMS OR (Transcranial OR brain) Magnetic Stimulation) AND TS = ('Electric Field$' OR 'Volume Conductor$' OR 'induced current density') AND TS = (('Head$' OR Anatomic* OR Brain OR Cortical OR Spher*) NEAR/5 (Comput* OR Model* OR Simulation$ OR Biophysical))					
Identified from database	104	Excluded (not relevant)	38	Identified from other sources	0	Relevant 66
Included in analysis	66					
3.3. Electrical conductivity: anisotropy						
Search data	TI = (TMS OR rTMS OR (Transcranial OR brain) Magnetic Stimulation) AND TS = ('Electric Field$' OR 'Volume Conductor$' OR 'induced current density') AND TS = ('Head$' OR Anatomic* OR Brain OR Cortical OR Spher*) AND TS = (Anisotropy)					
Identified from database	18	Excluded (not relevant)	14	Identified from other sources	0	Relevant 4
Included in analysis	4					
3.4. TMS coil models and verification						
Search data	TI = (TMS OR rTMS OR (Transcranial OR brain) Magnetic Stimulation) AND TS = ('Electric Field$' OR 'Volume Conductor$' OR 'induced current density') AND TS = ('Head$' OR Anatomic* OR Brain OR Cortical OR Spher*) AND TS = ('coil model*' OR 'coil wir*' OR (measure* OR validat* OR accura*) NEAR/4 (coil$))					
Identified from database	24	Excluded (not relevant)	17	Identified from other sources	0	Relevant 7
Included in analysis	7					
3.5 Effects of anatomical and inter-individual factors						
Search data	TI = (TMS OR rTMS OR (Transcranial OR brain) Magnetic Stimulation) AND TS = ('Electric Field$' OR 'Volume Conductor') AND TS = (('Head$' OR Anatomic* OR Brain OR Cortical) NEAR/5 (Comput* OR Model* OR Simulation$ OR Biophysical)) AND TS = ((gyrus OR gyral OR sulcus OR sulci OR variability OR individual$ OR subject$))					
Identified from database	52	Excluded (not relevant)	43	Identified from other sources	1	Relevant 9
Included in analysis	10					
3.6 Coil design: optimisation and performance						
Search data	TI = (TMS OR rTMS OR (Transcranial OR brain) Magnetic Stimulation) AND TS = ('Electric Field$' OR 'Volume Conductor') AND TS = (('Head$' OR Anatomic* OR Brain OR Cortical) NEAR/5 (Comput* OR Model* OR Simulation$ OR Biophysical))					

Table A1. Continued.

	AND TS = (coil AND (design OR optimization OR performance))						
Identified from database	48	Excluded (not relevant)	26	Identified from other sources	1	Relevant	22
Included in analysis	23						
	3.7 Guiding TMS dose						
Search data	TI = (TMS OR rTMS OR (Transcranial OR brain) Magnetic Stimulation) AND TS = ('Electric Field$' OR 'Volume Conductor') AND TS = (('Head$' OR Anatomic* OR Brain OR Cortical) NEAR/5 (Comput* OR Model* OR Simulation$ OR Biophysical)) AND TS = (guide OR atlas OR target* OR coil-target distance)						
Identified from database	39	Excluded (not relevant)	34	Identified from other sources	1	Relevant	5
Included in analysis	6						
	3.8 Localising TMS						
Search data	TI = (TMS OR rTMS OR 'Transcranial Magnetic Stimulation') AND TS = ('Electric Field$' OR 'Volume Conductor') AND TS = (('Head$' OR Anatomic* OR Brain OR Cortical) NEAR/5 (Comput* OR Model* OR Simulation$ OR Biophysical)) AND TS = ((physiologic* OR Electrophysiolog*) AND measureme* OR MEP OR fMRI OR PET OR DES OR 'motor threshold$')						
Identified from database	27	Excluded (not relevant)	16	Identified from other sources	1	Relevant	11
Included in analysis	12						
	4. Nerve modelling						
Search data	TI = (TMS OR 'Magnetic Stimulation' OR electromagnetic OR 'Induced Electric Field$' OR 'Magnetic Field Stimulation') AND TS = ('Electric Field$' OR 'Volume Conductor') AND TS = (Brain$ OR Cortex OR Head$) AND TS = (('I-wave$' OR 'D-wave$' OR 'Neuron*' OR 'Interneuron' or Axon$ OR Nerve$ OR 'pyramidal' OR 'White Matter') NEAR/10 (Comput* OR Multiscale OR Model* OR Simulation$ OR Biophysical*))						
Identified from database	42	Excluded (not relevant)	27	Identified from other sources	3	Relevant	15
Included in analysis	18						

ORCID iDs

Jose Gomez-Tames https://orcid.org/0000-0003-1917-8979
Ilkka Laakso https://orcid.org/0000-0002-8162-1356
Akimasa Hirata https://orcid.org/0000-0001-8336-1140

References

Aberra A S, Peterchev A V and Grill W M 2018 Biophysically realistic neuron models for simulation of cortical stimulation *J. Neural. Eng.* **15** 66023

Aberra A S, Wang B, Grill W M and Peterchev A V 2020 Simulation of transcranial magnetic stimulation in head model with morphologically-realistic cortical neurons *Brain Stimul.* **13** 175–89

Aonuma S, Gomez-Tames J, Laakso I, Hirata A, Takakura T, Tamura M and Muragaki Y 2018 A high-resolution computational localization method for transcranial magnetic stimulation mapping *NeuroImage* **172** 85–93

Arabkheradmand G, Krieg T D, Salinas F S, Fox P T and Mogul D J 2019 Predicting TMS-induced activation in human neocortex using concurrent TMS/PET, finite element analysis and computational modeling *Biomed. Phys. Eng. Express* **5** 25028

Ashburner J and Friston K J 2005 Unified segmentation *NeuroImage* **26** 839–51

Barchanski A, Gersem H D, Gjonaj E and Weiland T 2005 Impact of the displacement current on low-frequency electromagnetic fields computed using high-resolution anatomy models *Phys. Med. Biol.* **50** N243–9

Barker A T, Jalinous R and Freeston I L 1985 Non-invasive magnetic stimulation of human motor cortex *Lancet* **1** 1106–7

Bijsterbosch J D, Barker A T, Lee K-H and Woodruff P W R 2012 Where does transcranial magnetic stimulation (TMS) stimulate? Modelling of induced field maps for some common cortical and cerebellar targets *Med. Biol. Eng. Comput.* **50** 671–81
Bohning D E, Shastri A, Nahas Z, Lorberbaum J P, Andersen S W, Dannels W R, Haxthausen E-U, Vincent D J and George M S 1998 Echoplanar BOLD fMRI of brain activation induced by concurrent transcranial magnetic stimulation *Invest. Radiol.* **33** 336–40
Bungert A *et al* 2017 Where does TMS stimulate the motor cortex? Combining electrophysiological measurements and realistic field estimates to reveal the affected cortex position *Cereb. Cortex* **27** 5083–94
Burger H C and Milaan J B 1943 Measurements of the specific resistance of the human body to direct current *Acta Med. Scand.* **114** 584–607
Çan M K, Laakso I, Nieminen J O, Murakami T and Ugawa Y 2018 Coil model comparison for cerebellar transcranial magnetic stimulation *Biomed. Phys. Eng. Express* **5** 15020
Chiu S and Ritchie J 1979 A quantitative description of membrane currents in rabbit myelinated nerve *J. Physiol.* **292** 149–66
Christ A, Kainz W and Hahn E 2010 The virtual family—development of surface-based anatomical models of two adults and two children for dosimetric simulations *Phys. Med. Biol.* **55**
Cohen L G, Roth B J, Nilsson J, Dang N, Panizza M, Bandinelli S, Friauf W and Hallett M 1990 Effects of coil design on delivery of focal magnetic stimulation. Technical considerations *Electroencephalogr. Clin. Neurophysiol.* **75** 350–7
Crowther L J, Hadimani R L and Jiles D C 2014 Effect of anatomical brain development on induced electric fields during transcranial magnetic stimulation *IEEE Trans. Magn.* **50** 1–4
Dale A M, Fischl B and Sereno M I 1999 Cortical surface-based analysis *NeuroImage* **9** 179–94
Danner S M, Hofstoetter U S, Ladenbauer J, Rattay F and Minassian K 2011 Can the human lumbar posterior columns be stimulated by transcutaneous spinal cord stimulation? A modeling study *Artif. Organs* **35** 257–62
Dawson T and Stuchly M 1996 Analytic validation of a three-dimensional scalar-potential finite-difference code for low-frequency magnetic induction *Appl. Comput. Electromagn. Soc. J.* **11** 72–81
De Geeter N, Crevecoeur G, Dupré L, Van Hecke W and Leemans A 2012 A DTI-based model for TMS using the independent impedance method with frequency-dependent tissue parameters. *Phys. Med. Biol.* **57** 2169–88
De Geeter N, Crevecoeur G, Leemans A and Dupré L 2015 Effective electric fields along realistic DTI-based neural trajectories for modelling the stimulation mechanisms of TMS *Phys. Med. Biol.* **60** 453–71
De Geeter N, Lioumis P, Laakso A, Crevecoeur G and Dupré L 2016 How to include the variability of TMS responses in simulations: a speech mapping case study *Phys. Med. Biol.* **61** 7571–85
De Lucia M, Parker G J M, Embleton K, Newton J M and Walsh V 2007 Diffusion tensor MRI-based estimation of the influence of brain tissue anisotropy on the effects of transcranial magnetic stimulation *NeuroImage* **36** 1159–70
Deng Z-D, Lisanby S H and Peterchev A V 2013 Electric field depth–focality tradeoff in transcranial magnetic stimulation: simulation comparison of 50 coil designs *Brain Stimul.* **6** 1–13
Deng Z-D, Lisanby S H and Peterchev A V 2014 Coil design considerations for deep transcranial magnetic stimulation *Clin. Neurophysiol.* **125** 1202–12
Di Lazzaro V *et al* 2004 The physiological basis of transcranial motor cortex stimulation in conscious humans *Clin. Neurophysiol.* **115** 255–66
Dimbylow P J 1997 FDTD calculations of the whole-body averaged SAR in an anatomically realistic voxel model of the human body from 1 MHz to 1 GHz *Phys. Med. Biol.* **42** 479–90
Doheny E P *et al* 2008 The effect of subcutaneous fat thickness on the efficacy of transcutaneous electrical stimulation *Proc. 30th Annual Int. Conf. of the IEEE Engineering in Medicine and Biology Society EMBS 2008* pp 5684–7
Eaton H 1992 Electric field induced in a spherical volume conductor from arbitrary coils: application to magnetic stimulation and MEG *Med. Biol. Eng. Comput.* **30** 433–40
Esser S K, Hill S and Tononi G 2009 Breakdown of effective connectivity during slow wave sleep: investigating the mechanism underlying a cortical gate using large-scale modeling *J. Neurophysiol.* **102** 2096–111
Ferguson A S and Stroink G 1997 Factors affecting the accuracy of the boundary element method in the forward problem-I: calculating surface potentials *IEEE Trans. Biomed. Eng.* **44** 1139–55
Fischl B 2012 FreeSurfer *NeuroImage* **62** 774–81
Frankenhaeuser B and Huxley A F 1964 The action potential in the myelinated nerve fiber of xenopus laevis as computed on the basis of voltage clamp data *J. Physiol.* **171** 302–15
Gabriel S, Lau R and Gabriel C 1996 The dielectric properties of biological tissues: II. Measurements in the frequency range 10 Hz to 20 GHz *Phys. Med. Biol.* **41** 2251
Gomez L J, Dannhauer M, Koponen L M and Peterchev A V 2020 Conditions for numerically accurate TMS electric field simulation *Brain Stimul.* **13** 157–66
Gomez L J, Goetz S M and Peterchev A V 2018 Design of transcranial magnetic stimulation coils with optimal trade-off between depth, focality, and energy *J. Neural. Eng.* **15** 46033
Gomez-Tames J *et al* 2019 Brain cortical stimulation thresholds to different magnetic field sources exposures at intermediate frequencies *IEEE Trans. Electromagn. Compat.* **61** 1944–52
Gomez-Tames J, Hamasaka A, Hirata A, Laakso I, Lu M and Ueno S 2020a Group-level analysis of induced electric field in deep brain regions by different TMS coils *Phys. Med. Biol.* **65** 025007
Gomez-Tames J, Hamasaka A, Laakso I, Hirata A and Ugawa Y 2018 Atlas of optimal coil orientation and position for TMS: a computational study *Brain Stimul.* **11** 839–48
Gomez-Tames J, Laakso I, Murakami T, Ugawa Y and Hirata A 2020b TMS activation site estimation using multiscale realistic head models *J. Neural. Eng.* **17** 36004
Goodwin B D and Butson C R 2015 Subject-specific multiscale modeling to investigate effects of transcranial magnetic stimulation *Neuromodulation: Technol. Neural Interface* **18** 694–704
Guadagnin V, Parazzini M, Fiocchi S, Liorni I and Ravazzani P 2016 Deep transcranial magnetic stimulation: modeling of different coil configurations *IEEE Trans. Biomed. Eng.* **63** 1543–50
Hernandez-Garcia L, Hall T, Gomez L and Michielssen E 2010 A numerically optimized active shield for improved transcranial magnetic stimulation targeting *Brain Stimul.* **3** 218–25
Hirata A, Ito F and Laakso I 2013 Confirmation of quasi-static approximation in SAR evaluation for a wireless power transfer system *Phys. Med. Biol.* **58** N241–9
Hodgkin A L and Huxley A F 1952 A quantitative description of membrane current and its application to conduction and excitation in nerve *Bull. Math. Biol.* **117** 23–25

Holsheimer J *et al* 2007 Cathodal, anodal or bifocal stimulation of the motor cortex in the management of chronic pain? *Acta Neurochir. Suppl.* **97** 57–66
Huang Y, Datta A, Bikson M and Parra L C 2019 Realistic volumetric-approach to simulate transcranial electric stimulation-ROAST-a fully automated open-source pipeline *J. Neural. Eng.* **16** 56006
Hyodo A and Ueno S 1996 Nerve excitation model for localized magnetic stimulation of finite neuronal structures *IEEE Trans. Magn.* **32** 5112–4
IEEE Std C95.1-2019 2019 *IEEE Standard for Safety Levels with respect to Human Exposure to Electric, Magnetic, and Electromagnetic Fields, 0 Hz to 300 GHz*
Im C H and Lee C 2006 Computer-aided performance evaluation of a multichannel transcranial magnetic stimulation system *IEEE Trans. Magn.* **42** 3803–8
International Commission on Non-Ionizing Radiation Protection 2020 Guidelines for limiting exposure to electromagnetic fields (100 kHz to 300 GHz) *Health Phys.* **118** 483–524
Iwahashi M, Gomez-Tames J, Laakso I and Hirata A 2017 *Evaluation method for in situ* electric field in standardized human brain for different transcranial magnetic stimulation coils *Phys. Med. Biol.* **62** 2224–38
Jackson J D and Fox R F 1999 Classical electrodynamics, 3rd edn *Am. J. Phys.* **67** 841–2
Janssen A and Oostendorp T 2015 The coil orientation dependency of the electric field induced by TMS for M1 and other brain areas *J. Neuroeng. Rehabil.* **12** 47
Janssen A M, Oostendorp T F and Stegeman D F 2014 The effect of local anatomy on the electric field induced by TMS: evaluation at 14 different target sites *Med. Biol. Eng. Comput.* **52** 873–83
Janssen A M, Rampersad S M, Lucka F, Lanfer B, Lew S, Aydin Ü, Wolters C H, Stegeman D F and Oostendorp T F 2013 The influence of sulcus width on simulated electric fields induced by transcranial magnetic stimulation *Phys. Med. Biol.* **58** 4881–96
Çan M K *et al* 2019 *Biomed. Phys. Eng. Express* **5** 015020
Kamitani Y, Bhalodia V M, Kubota Y and Shimojo S 2001 A model of magnetic stimulation of neocortical neurons *Neurocomputing* **38–40** 697–703
Kim D H, Georghiou G E and Won C 2006 Improved field localization in transcranial magnetic stimulation of the brain with the utilization of a conductive shield plate in the stimulator *IEEE Trans. Biomed. Eng.* **53** 720–5
Koponen L M, Nieminen J O and Ilmoniemi R J 2015 Minimum-energy coils for transcranial magnetic stimulation: application to focal stimulation *Brain Stimul.* **8** 124–34
Koponen L M, Nieminen J O, Mutanen T P, Stenroos M and Ilmoniemi R J 2017 Coil optimisation for transcranial magnetic stimulation in realistic head geometry *Brain Stimul.* **10** 795–805
Krieg T D, Salinas F S, Narayana S, Fox P T and Mogul D J 2015 Computational and experimental analysis of TMS-induced electric field vectors critical to neuronal activation *J. Neural. Eng.* **12** 46014
Laakso I and Hirata A 2012 Fast multigrid-based computation of the induced electric field for transcranial magnetic stimulation *Phys. Med. Biol.* **57** 7753–65
Laakso I, Hirata A and Ugawa Y 2014 Effects of coil orientation on the electric field induced by TMS over the hand motor area *Phys. Med. Biol.* **59** 203–18
Laakso I, Murakami T, Hirata A and Ugawa Y 2018 Where and what TMS activates: experiments and modeling *Brain Stimul.* **11** 166–74
Laakso I, Tanaka S, Koyama S, De Santis V and Hirata A 2015 Inter-subject variability in electric fields of motor cortical tDCS *Brain Stimul.* **8** 906–13
Lazzaro V, Oliviero A, Mazzone P, Insola A, Pilato F, Saturno E, Accurso A, Tonali P and Rothwell J 2001 Comparison of descending volleys evoked by monophasic and biphasic magnetic stimulation of the motor cortex in conscious humans *Exp. Brain Res.* **141** 121–7
Lee E G *et al* 2016 Investigational effect of brain-scalp distance on the efficacy of transcranial magnetic stimulation treatment in depression *IEEE Trans. Magn.* **52** 1–4
Li B, Virtanen J P, Oeltermann A, Schwarz C, Giese M A, Ziemann U and Benali A 2017 Lifting the veil on the dynamics of neuronal activities evoked by transcranial magnetic stimulation *eLife* **6** e30552
Li C, Liu C, Yang L, He L and Wu T 2019 Particle swarm optimization for positioning the coil of transcranial magnetic stimulation *Biomed. Res. Int.* **2019** 9461018
Lu M and Ueno S 2015a Computational study toward deep transcranial magnetic stimulation using coaxial circular coils *IEEE Trans. Biomed. Eng.* **62** 2911–9
Lu M and Ueno S 2015b Deep transcranial magnetic stimulation using figure-of-eight and halo coils *IEEE Trans. Magn.* **51** 1–4
Lu M and Ueno S 2017 Comparison of the induced fields using different coil configurations during deep transcranial magnetic stimulation *PLoS One* **12** e0178422
Lu M, Ueno S, Thorlin T and Persson M 2009 Calculating the current density and electric field in human head by multichannel transcranial magnetic stimulation *IEEE Trans. Magn.* **45** 1662–5
Makarov S N, Noetscher G M, Raij T and Nummenmaa A 2018 A quasi-static boundary element approach with fast multipole acceleration for high-resolution bioelectromagnetic models *IEEE Trans. Biomed. Eng.* **65** 2675–83
McIntyre C C, Richardson A G and Grill W M 2002 Modeling the excitability of mammalian nerve fibers: influence of afterpotentials on the recovery cycle *J. Neurophysiol.* **87** 995–1006
McNeal D 1976 Analysis of a model for excitation of myelinated nerve *IEEE Trans. Biomed. Eng.* **4** 329–37
Mikkonen M, Laakso I, Sumiya M, Koyama S, Hirata A and Tanaka S 2018 TMS motor thresholds correlate with TDCS electric field strengths in hand motor area *Front. Neurosci.* **12** 426
Miranda P, Hallett M and Basser P 2003 The electric field induced in the brain by magnetic stimulation: a 3-D finite-element analysis of the effect of tissue heterogeneity and anisotropy *IEEE Trans. Biomed. Eng.* **50** 1074–85
Moezzi B, Schaworonkow N, Plogmacher L, Goldsworthy M R, Hordacre B, McDonnell M D, Iannella N, Ridding M C and Triesch J 2018 Simulation of electromyographic recordings following transcranial magnetic stimulation *J. Neurophysiol.* **120** 2532–41
Mueller J K *et al* 2014 Simultaneous transcranial magnetic stimulation and single-neuron recording in alert non-human primates *Nat. Neurosci.* **17** 1130–6
Nagaoka T, Watanabe S, Sakurai K, Kunieda E, Watanabe S, Taki M and Yamanaka Y 2004 Development of realistic high-resolution whole-body voxel models of Japanese adult males and females of average height and weight, and application of models to radio-frequency electromagnetic-field dosimetry *Phys. Med. Biol.* **49** 1–15
Nagarajan S S and Durand D M 1996 A generalized cable equation for magnetic stimulation of axons *IEEE Trans. Biomed. Eng.* **43** 304–12

Nagarajan S S, Durand D M and Hsuing-Hsu K 1997 Mapping location of excitation during magnetic stimulation: effects of coil position *Ann. Biomed. Eng.* **25** 112–25
Nagarajan S S, Durand D M and Warman E N 1993 Effects of induced electric fields on finite neuronal structures: a simulation study *IEEE Trans. Biomed. Eng.* **40** 1175–88
Nicholson P W 1965 Specific impedance of cerebral white matter *Exp. Neurol.* **13** 386–401
Nieminen J O, Koponen L M and Ilmoniemi R J 2015 Experimental characterization of the electric field distribution induced by TMS devices *Brain Stimul.* **8** 582–9
Nummenmaa A, McNab J A, Savadjiev P, Okada Y, Hämäläinen M S, Wang R, Wald L L, Pascual-Leone A, Wedeen V J and Raij T 2014 Targeting of white matter tracts with transcranial magnetic stimulation *Brain Stimul.* **7** 80–84
Nummenmaa A, Stenroos M, Ilmoniemi R J, Okada Y C, Hämäläinen M S and Raij T 2013 Comparison of spherical and realistically shaped boundary element head models for transcranial magnetic stimulation navigation *Clin. Neurophysiol.* **124** 1995–2007
O'Reardon J P *et al* 2007 Efficacy and safety of transcranial magnetic stimulation in the acute treatment of major depression: a multisite randomized controlled trial *Biol. Psychiatry* **62** 1208–16
Opitz A, Falchier A, Linn G S, Milham M P and Schroeder C E 2017 Limitations of ex vivo measurements for in vivo neuroscience *Proc. Natl Acad. Sci. USA* **114** 5243–6
Opitz A, Fox M D, Craddock R C, Colcombe S and Milham M P 2016 An integrated framework for targeting functional networks via transcranial magnetic stimulation *NeuroImage* **127** 86–96
Opitz A, Legon W, Rowlands A, Bickel W K, Paulus W and Tyler W J 2013 Physiological observations validate finite element models for estimating subject-specific electric field distributions induced by transcranial magnetic stimulation of the human motor cortex *NeuroImage* **81** 253–64
Opitz A, Windhoff M, Heidemann R M, Turner R and Thielscher A 2011 How the brain tissue shapes the electric field induced by transcranial magnetic stimulation *NeuroImage* **58** 849–59
Opitz A, Zafar N, Bockermann V, Rohde V and Paulus W 2014 Validating computationally predicted TMS stimulation areas using direct electrical stimulation in patients with brain tumors near precentral regions *Neuroimage Clin.* **4** 500–7
Ottenhausen M, Krieg S M, Meyer B and Ringel F 2015 Functional preoperative and intraoperative mapping and monitoring: increasing safety and efficacy in glioma surgery *Neurosurg. Focus* **38** E3
Park J S, Jung Y W, Choi H-D and Lee A-K 2018 VK-phantom male with 583 structures and female with 459 structures, based on the sectioned images of a male and a female, for computational dosimetry *J. Radiat. Res.* **59** 338–80
Pashut T, Wolfus S, Friedman A, Lavidor M, Bar-Gad I, Yeshurun Y and Korngreen A 2011 Mechanisms of magnetic stimulation of central nervous system neurons *PLoS Comput. Biol.* **7** e1002022
Perera T, George M S, Grammer G, Janicak P G, Pascual-Leone A and Wirecki T S 2016 The clinical TMS society consensus review and treatment recommendations for TMS therapy for major depressive disorder *Brain Stimul.* **9** 336–46
Petrov P I, Mandija S, Sommer I E C, van den Berg C A T and Neggers S F W 2017 How much detail is needed in modeling a transcranial magnetic stimulation figure-8 coil: measurements and brain simulations *PLoS One* **12** e0178952
Plonsey R and Heppner D 1967 Considerations of quasi-stationarity in electrophysiological systems *Bull. Math. Biophys.* **29** 657–64
Rashed E A, Gomez-Tames J and Hirata A 2019 Development of accurate human head models for personalized electromagnetic dosimetry using deep learning *NeuroImage* **202** 116132
Rashed E A, Gomez-Tames J and Hirata A 2020a Deep learning-based development of personalized human head model with non-uniform conductivity for brain stimulation *IEEE Trans. Med. Imaging* **39** 2351–62
Rashed E A, Gomez-Tames J and Hirata A 2020b End-to-end semantic segmentation of personalized deep brain structures for non-invasive brain stimulation *Neural Netw.* (https://doi.org/10.1016/j.neunet.2020.02.006)
Rastogi P, Tang Y, Zhang B, Lee E G, Hadimani R L and Jiles D C 2017 Quadruple butterfly coil with passive magnetic shielding for focused transcranial magnetic stimulation *IEEE Trans. Magn.* **53**
Rattay F 1986 Analysis of models for external stimulation of axons *IEEE Trans. Biomed. Eng.* **10** 974–7
Ravazzani P, Ruohonen J, Grandori F and Tognola G 1996 Magnetic stimulation of the nervous system: induced electric field in unbounded, semi-infinite, spherical, and cylindrical media *Ann. Biomed. Eng.* **24** 606–16
Reijonen J, Säisänen L, Könönen M, Mohammadi A and Julkunen P 2020 The effect of coil placement and orientation on the assessment of focal excitability in motor mapping with navigated transcranial magnetic stimulation *J. Neurosci. Methods* **331** 108521
Reilly J P 1989 Peripheral nerve stimulation by induced electric currents: exposure to time-varying magnetic fields *Med. Biol. Eng. Comput.* **27** 101–10
Rossi S, Hallett M, Rossini P M and Pascual-Leone A 2009 Safety, ethical considerations, and application guidelines for the use of transcranial magnetic stimulation in clinical practice and research *Clin. Neurophysiol.* **120** 2008–39
Roth B J and Basser P J 1990 A model of the stimulation of a nerve fiber by electromagnetic induction *IEEE Trans. Biomed. Eng.* **37** 588–97
Roth Y, Zangen A and Hallett M 2002 A coil design for transcranial magnetic stimulation of deep brain regions *J. Clin. Neurophysiol.* **19** 361–70
Salinas F S, Lancaster J L and Fox P T 2007 Detailed 3D models of the induced electric field of transcranial magnetic stimulation coils *Phys. Med. Biol.* **52** 2879–92
Salinas F S, Lancaster J L and Fox P T 2009 3D modeling of the total electric field induced by transcranial magnetic stimulation using the boundary element method *Phys. Med. Biol.* **54** 3631–47
Salvador R, Miranda P C, Roth Y and Zangen A 2009 High permeability cores to optimize the stimulation of deeply located brain regions using transcranial magnetic stimulation *Phys. Med. Biol.* **54** 3113–28
Salvador R, Silva S, Basser P J and Miranda P C 2011 Determining which mechanisms lead to activation in the motor cortex: a modeling study of transcranial magnetic stimulation using realistic stimulus waveforms and sulcal geometry *Clin. Neurophysiol.* **122** 748–58
Samoudi A M, Tanghe E, Martens L and Joseph W 2018 Deep transcranial magnetic stimulation: improved coil design and assessment of the induced fields using MIDA model *Biomed. Res. Int.* **2018** 1–9
Saturnino G B, Madsen K H and Thielscher A 2019 Electric field simulations for transcranial brain stimulation using FEM: an efficient implementation and error analysis *J. Neural. Eng.* **16** 66032
Sekino M, Ohsaki H, Takiyama Y, Yamamoto K, Matsuzaki T, Yasumuro Y, Nishikawa A, Maruo T, Hosomi K and Saitoh Y 2015 Eccentric figure-eight coils for transcranial magnetic stimulation *Bioelectromagnetics* **36** 55–65
Sendra-Balcells C *et al* 2020 Convolutional neural network MRI segmentation for fast and robust optimization of transcranial electrical current stimulation of the human brain bioRxiv 2020.01.29.924985 (https://doi.org/10.1101/2020.01.29.924985)

Seo H, Kim D and Jun S C 2015 Computational study of subdural cortical stimulation: effects of simulating anisotropic conductivity on activation of cortical neurons *PLoS One* **10** e0128590
Seo H, Schaworonkow N, Jun S C and Triesch J 2017 A multi-scale computational model of the effects of TMS on motor cortex *F1000Research* **5** 1945
Seynaeve L, Haeck T, Gramer M, Maes F, De Vleeschouwer S and Van Paesschen W 2019 Optimized preoperative motor cortex mapping in brain tumors using advanced processing of transcranial magnetic stimulation data *Neuroimage Clin.* **21** 101657
Silva S, Basser P J and Miranda P C 2008 Elucidating the mechanisms and loci of neuronal excitation by transcranial magnetic stimulation using a finite element model of a cortical sulcus *Clin. Neurophysiol.* **119** 2405–13
Smith S M 2002 Fast robust automated brain extraction *Hum. Brain Mapp.* **17** 143–55
Soldati M and Laakso I 2020 Computational errors of the induced electric field in voxelized and tetrahedral anatomical head models exposed to spatially uniform and localized magnetic fields *Phys. Med. Biol.* **65** 15001
Soldati M, Mikkonen M, Laakso I, Murakami T, Ugawa Y and Hirata A 2018 A multi-scale computational approach based on TMS experiments for the assessment of electro-stimulation thresholds of the brain at intermediate frequencies *Phys. Med. Biol.* **63** 225006
Stenroos M and Koponen L M 2019 Real-time computation of the TMS-induced electric field in a +realistic head model *NeuroImage* **203** 116159
Stokes M G, Barker A T, Dervinis M, Verbruggen F, Maizey L, Adams R C and Chambers C D 2013 Biophysical determinants of transcranial magnetic stimulation: effects of excitability and depth of targeted area *J. Neurophysiol.* **109** 437–44
Sweeney J D, Mortimer J T and Durand D 1987 Modeling of mammalian myelinated nerve for functional neuromuscular electrostimulation *IEEE 97th Annual Conf. Eng. Med. Biol. Soc., Boston* **9** 1577–8
Tachas N J, Efthimiadis K G and Samaras T 2013 The effect of coil modeling on the predicted induced electric field distribution during TMS *IEEE Trans. Magn.* **49** 1096–100
Taniguchi M, Cedzich C and Schramm J 1993 Modification of cortical stimulation for motor evoked potentials under general anesthesia: technical description *Neurosurgery* **32** 219–26
Terao Y and Ugawa Y 2002 Basic mechanisms of TMS *J. Clin. Neurophysiol.* **19** 322–43
Thielscher A and Kammer T 2002 Linking physics with physiology in TMS: a sphere field model to determine the cortical stimulation site in TMS *NeuroImage* **17** 1117–30
Thielscher A and Kammer T 2004 Electric field properties of two commercial figure-8 coils in TMS: calculation of focality and efficiency *Clin. Neurophysiol.* **115** 1697–708
Thielscher A, Opitz A and Windhoff M 2011 Impact of the gyral geometry on the electric field induced by transcranial magnetic stimulation *NeuroImage* **54** 234–43
Tischler H, Wolfus S, Friedman A, Perel E, Pashut T, Lavidor M, Korngreen A, Yeshurun Y and Bar-Gad I 2011 Mini-coil for magnetic stimulation in the behaving primate *J. Neurosci. Methods* **194** 242–51
Tofts P S 1990 The distribution of induced currents in magnetic stimulation of the nervous system *Phys. Med. Biol.* **35** 1119–28
Toschi N, Welt T, Guerrisi M and Keck M E 2008 A reconstruction of the conductive phenomena elicited by transcranial magnetic stimulation in heterogeneous brain tissue *Phys. Medica* **24** 80–86
Ueno S, Tashiro T and Harada K 1988 Localized stimulation of neural tissues in the brain by means of a paired configuration of time-varying magnetic fields *J. Appl. Phys.* **64** 5862–4
Vöröslakos M *et al* 2018 Direct effects of transcranial electric stimulation on brain circuits in rats and humans *Nat. Commun.* **9** 483
Wagner T A, Zahn M, Grodzinsky A J and Pascual-Leone A 2004 Three-dimensional head model simulation of transcranial magnetic stimulation *IEEE Trans. Biomed. Eng.* **51** 1586–98
Wang B, Grill W M and Peterchev A V 2018a Coupling magnetically induced electric fields to neurons: longitudinal and transverse activation *Biophys. J.* **115** 95–107
Wang B, Shen M R, Deng Z-D, Smith J E, Tharayil J J, Gurrey C J, Gomez L J and Peterchev A V 2018b Redesigning existing transcranial magnetic stimulation coils to reduce energy: application to low field magnetic stimulation *J. Neural. Eng.* **15** 36022
Wang W and Eisenberg S R 1994 A three-dimensional finite element method for computing magnetically induced currents in tissues *IEEE Trans. Magn.* **30** 5015–23
Wei X, Li Y, Lu M, Wang J and Yi G 2017 Comprehensive survey on improved focality and penetration depth of transcranial magnetic stimulation employing multi-coil arrays *Int. J. Environ. Res. Public Health* **14**
Weise K, Numssen O, Thielscher A, Hartwigsen G and Knösche T R 2020 A novel approach to localize cortical TMS effects *NeuroImage* **209** 116486
Windhoff M, Opitz A and Thielscher A 2013 Electric field calculations in brain stimulation based on finite elements: an optimized processing pipeline for the generation and usage of accurate individual head models *Hum. Brain Mapp.* **34** 923–35
Wongsarnpigoon A and Grill W M 2008 Computational modeling of epidural cortical stimulation *J. Neural. Eng.* **5** 443–54
Wu T, Fan J, Lee K S and Li X 2016 Cortical neuron activation induced by electromagnetic stimulation: a quantitative analysis via modelling and simulation *J. Comput. Neurosci.* **40** 51–64
Wu Y *et al* 2012 Creation of a female and male segmentation dataset based on Chinese visible human (CVH) *Comput. Med. Imaging Graph.* **36** 336–42
Yamamoto K, Suyama M, Takiyama Y, Kim D, Saitoh Y and Sekino M 2015 Characteristics of bowl-shaped coils for transcranial magnetic stimulation *J. Appl. Phys.* **117** 17A318
Yamamoto K, Takiyama Y, Saitoh Y and Sekino M 2016 Numerical analyses of transcranial magnetic stimulation based on individual brain models by using a scalar-potential finite-difference method *IEEE Trans. Magn.* **52**
Yamamoto T and Yamamoto Y 1976 Electrical properties of the epidermal stratum corneum *Med. Biol. Eng.* **14** 151–8
Yokota T, Maki T, Nagata T, Murakami T, Ugawa Y, Laakso I, Hirata A and Hontani H 2019 Real-time estimation of electric fields induced by transcranial magnetic stimulation with deep neural networks *Brain Stimul.* **12** 1500–7
Zhong X, Rastogi P, Wang Y, Lee E G and Jiles D 2019 Investigating the role of coil designs and anatomical variations in cerebellar TMS *IEEE Trans. Magn.* **55** 1–5
Zubal I G, Harrell C R, Smith E O, Rattner Z, Gindi G and Hoffer P B 1994 Computerized three-dimensional segmented human anatomy *Med. Phys.* **21** 299–302